Simulating the Effects of Climate Change on Fraser River Flood Scenarios – Phase 2

Final Report

26 May 2015

Prepared for:
Flood Safety Section
Ministry of Forests Lands and Natural Resource Operations

Rajesh R. Shrestha
Markus A. Schnorbus
Alex J. Cannon
Francis W. Zwiers

Simulating the Effects of Climate Change on Fraser River Flood Scenarios – Phase 2

EXECUTIVE SUMMARY

Projecting streamflow extremes under nonstationarity is important for managing river flooding in a changing climate. The objective of this study is to develop a nonstationary modelling framework for projecting future changes in the annual exceedance probabilities of streamflow extremes for the Fraser River at Hope station (WSC gauge 08MF005) using phase 5 of the Coupled Model Intercomparison Project (CMIP5) generation of global climate models (GCMs). Nonstationarity is represented by the variable parameter Generalized Extreme Value (GEV) distribution, which provides a flexible approach for estimating the distribution of extremes.

In the first part of this work, a stationary analysis of extreme historical discharge was conducted based on 102-year (1912-2013) historical annual maximum daily flow data, supplemented with the estimated 1894 peak discharge value. Based on the fitted Gumbel distribution, the 1894 event (≈ 17000 m^3/s) has a return period of about 500 years, with a confidence range (5% to 95%) of 16000 m^3/s to 18000 m^3/s. Likewise, an event of 17000 m^3/s has a return period that ranges from 250 to 1000 years.

In the second part of this study, a nonstationary flood frequency analysis was conducted with the parameters of the GEV distribution expressed as a function of climate covariates. The parameters were estimated using the GEV conditional density network (GEVcdn) with seasonal precipitation and temperature, which drive the peak streamflow in spring, and time (year) used as covariates. The GEVcdn model was trained using climate projections and hydrology model output based on the phase 3 of the Coupled Model Intercomparison Project (CMIP3). The results of the GEVcdn nonstationary model showed a good ability of the model to simulate quantile discharges. We then projected future flow quantiles by using covariates taken from latest CMIP5 generation of climate projections. For the evaluation of the future changes in discharge quantiles, we considered 30-year periods as stationary, and future change in discharge quantiles were evaluated relative to the historical discharge quantiles (from the first part of this study).

The future discharge quantiles for the CMIP5-based projections mostly showed increases in flow magnitudes for the three representative concentration pathways (RCPs)[1] and three future periods. In general, the larger the return period, the larger is the increase in flow magnitude. The median increases in 2071-2100 based on CMIP5 GCM ensembles are 5% to 15%, 3% to 18% and -3% to 24% (range are for 10 year-10000 year return periods) for RCP 2.6, 4.5 and 8.5, respectively. The maximum increases in 2071-2098 from CMIP5 GCM ensembles are 15% to 53%, 21% to 52% and 22% to 74% for RCP 2.6, 4.5 and 8.5, respectively. The results of this study are affected by a number of different sources of uncertainties, which arise from the data and model used. In particular, long return periods (e.g. > 1000 year) are affected by uncertainties due to sampling variability, and the results for long return period events presented in this report should be treated with a caution.

[1] Emissions scenarios are summarized in Appendix A

1. INTRODUCTION

1.1 Project Background

The Flood Safety Section of the Ministry of Forests, Lands and Natural Resource Operations (FLNRO) and Northwest Hydraulic Consultants (NHC) completed a joint project on: "Simulating the Effects of Sea Level Rise and Climate Change on Fraser River Flood Scenarios" (Flood Safety Section, 2014). The project used the MIKE-11 hydrodynamic model for the Fraser River from Hope to the Strait of Georgia to generate water surface profiles for peak flow quantiles corresponding to a range of annual exceedance probabilities (AEPs) derived from historical flow data. Additionally, future water surface profiles for the same range of AEPs were generated, with the future discharge quantiles derived from the Pacific Climate Impacts Consortium's (PCIC's) projected future hydrologic scenarios (Shrestha et al. 2012) based on the Variable Infiltration Capacity (VIC) hydrology model simulations. These simulations were based on climate projections using Global Climate Models (GCMs) and emissions scenarios from phase 3 of the Coupled Model Intercomparison Project (CMIP3)[2].

The purpose of the current study is to update the peak flow quantile projections for the Fraser River at Hope using climate projections from the more recent phase 5 of the Coupled Model Intercomparison Project (CMIP5). These peak flow projections will be based on results from a new generation of GCMs and new emissions scenarios (Appendix A provides a description of the CMIP3 and CMIP5 emissions scenarios). Given the projected intensification of the global water cycle due to climate change (Huntington 2006) and natural climate variability, another important consideration for generating future change in discharge extremes is nonstationarity. This study explicitly considers nonstationarity by using a variable parameter Generalized Extreme Value (GEV) distribution.

The direct means of estimating peak flow quantiles for given AEPs for CMIP5 would be to force VIC with the downscaled CMIP5 climate projections. However, CMIP5-based VIC projections are presently (April 2015) unavailable. Given the computational cost and time required for downscaling GCMs and hydrologic modelling, such a methodology was not considered for this study. As an alternative, a computationally efficient Generalized Extreme Value conditional density network (GEVcdn) model (Cannon 2010, 2011), which can estimate nonstationary discharge quantiles based on covariates, was employed. Climatic covariates derived from an ensemble of 23 CMIP3 projections were used to train the GEVcdn model to emulate the VIC simulated peak streamflows (Shrestha et al. 2012). The model was then used to estimate the streamflow peak flow quantiles for the CMIP5 generation of climate projections. Given that both CMIP3 and CMIP5 projections produced generally warmer and wetter future climate responses for the Fraser basin (Schnorbus and Cannon 2014), the CMIP3 data was considered suitable for training the GEVcdn model. Similar methodology - statistical emulation of the monthly streamflow projections for the CMIP3 GCMs and simulation of for CMIP5 GCMs - was used by Schnorbus and Cannon (2014).

[2]More information on the Coupled Model Intercomparison Project can be found at http://cmip-pcmdi.llnl.gov/index.html?submenuheader=0 (last accessed April 30, 2015)

1.2 Scope of Work

1.2.1. ***Setup of a stationary statistical model for the historical streamflow extremes data.*** The GEV distribution was fit to the historical data (1912-2013) augmented with historical peak discharge values composed of a single extreme flood magnitude.

1.2.2. Setup of a nonstationary statistical model for approximating the relationship between climate variables (i.e., precipitation and temperature) and streamflow extremes. After reviewing previous studies on statistical modelling of climate extremes (e.g., Kharin and Zwiers 2005; Cannon 2010; Zhang et al. 2010; Kharin et al. 2013; Vasiliades et al. 2014) and streamflow extremes (e.g., Towler et al. 2010; Salas and Obeysekera 2014; Condon et al. 2015), the GEVcdn nonstationary model was setup for linking the CMIP3 precipitation and temperature covariates with the VIC model simulated streamflow extremes for the Fraser River at Hope station that are extracted from VIC simulations driven with the same CMIP3 GCMs.

1.2.3. Evaluation of the performance of the nonstationary statistical model. A number of combinations of covariates were considered for modelling the streamflow extremes. After evaluating the performance of the different covariate combinations, the model with the best statistical performance was chosen.

1.2.4. Projection of future flow quantiles using statistical model. Using the nonstationary GEV statistical mode, peak flow quantiles were resampled from the 30-year baseline (1961-1990), and 30-year (2011-2040 and 2041-2070) and 28-year (2071-2098) future periods. GEV distributions were next fit to the resampled data assuming stationarity within each 30-year period. The baseline and future flood frequency distributions were then used to estimate the percentage change in future discharge quantiles for given AEPs. The percentage change values were then used to scale the historical discharge quantiles (section 1.2.1), thus obtaining estimates of projected future discharge quantiles.

1.3 Deliverables

Based on the project proposal, PCIC prepared this report by including the following deliverables:

- Annual maximum discharge data and plotting positions for the historical stationary flood frequency analysis.
- Model calibration and validation results for the nonstationary flood frequency analysis.
- Future flood frequency curves for the CMIP3 and CMIP5 GCMs for return periods extending from 10 to 10,000 years.

- A table showing percent change in projected discharges for 10-year, 50-year, 100-year, 200-year, 500-year, 1000-year, 2000-year, 5000-year, and 10000-year return periods (for Timespan1= 2011 to 2040, Timespan2= 2041 to 2070, and Timespan3= 2071 to 2098).
- A table with projected discharges for 10-year, 50-year, 100-year, 200-year, 500-year, 1000-year, 2000-year, 5000-year, and 10000-year return periods.
- Boxplots showing statistical distribution of discharges from multiple GCMs, emissions scenarios, and future periods.

2. METHODS

2.1 Generalized Extreme Value (GEV) Model

Extreme value theory provides a basis for modelling the maxima or minima of a data series. On the basis of an underlying asymptotic argument, the theory allows for extrapolation beyond observed events (Coles 2001; Towler et al. 2010) using the generalized extreme value (GEV) distribution. The cumulative distribution function (CDF) of the GEV can be expressed as:

$$F(x,\theta) = \exp\left[-\left\{1+\xi\left(\frac{x-\mu}{\sigma}\right)\right\}^{-1/\xi}\right] \tag{1}$$

for $\xi \neq 0,\ 1+\xi\left(\frac{x-\mu}{\sigma}\right) > 0$

$$F(x,\theta) = \exp\left[-\exp\left\{-\left(\frac{x-\mu}{\sigma}\right)\right\}\right] \tag{2}$$

for $\xi = 0$

where $\theta = (\mu, \sigma, \xi)$ are the location (μ), scale ($\sigma > 0$) and shape (ξ) parameters of the GEV distribution and *x* denotes the annual streamflow maximum value (in this case). The location and scale parameters represent the centre and spread of the distribution, respectively. Based on the shape parameter, which characterizes the distribution's tail, the GEV can assume three types: (I) $\xi = 0$ light-tailed or Gumbel type. (II) $\xi > 0$ heavy-tailed or Fréchet type; and (III) $\xi < 0$ bounded tail or Weibull type. Note that the parameterization of equations (1) and (2) follows the convention in Towler et al. (2010) – in the hydro-climatological literature it is also common to parameterize ξ^* = $-\xi$ (e.g., Kharin and Zwiers 2005; Cannon 2010).

From equations (1) and (2), the probabilistic quantile x_τ can be obtained:

$$x_\tau = \mu - \frac{\sigma}{\xi}\left[1 - \{-\log(\tau)\}^{-\xi}\right],\ \xi \neq 0 \tag{3}$$

$$x_\tau = \mu - \sigma log\{-log(\tau)\}, \qquad \xi = 0 \tag{4}$$

where τ is the non-exceedance probability with the exceedance probability $p = (1-\tau)$ and $0 < \tau < 1$, and the annual maxima (or minima) x_τ corresponds to the return period $T = 1/(1-\tau)$.

The distribution can represent either stationary or nonstationary conditions by using either constant or variables (one or more) GEV parameters, respectively. Nonstationary parameters can be described as functions of covariates. Under stationarity, a *T*-year event has two equivalent interpretations. The first interpretation is that the expected waiting time for an event until the next exceedance is *T*-years. The second interpretation is that the size of an event x_τ has probability 1/T of exceedence in any given year (Wilks 2006; Cooley 2013). In contrast, in the non-stationary case the return value becomes covariate dependent, and thus only the latter (instantaneous risk) interpretation is possible.

2.2 Stationary Analysis of Historical Extreme Discharge

Flood frequency analysis for the Fraser River at Hope (WSC gauge 08MF005) was conducted based on 102 observations of annual maximum daily discharge observed continuously from 1912 to 2013 (the instrumental record). This instrumental record can be augmented with documentary historical peak discharge values composed of a single extreme flood event in 1894 of estimated magnitude, and a further 64 years of data (1847 to 1911, excluding 1894) where the annual maximum discharge was known not to have exceeded the flood of 1894 (Northwest Hydraulic Consultants 2008). The annual maximum discharge values for 2014-2015 have not yet been published by Water Survey of Canada and the 2013 value is still considered provisional (Flood Safety Section 2014). The 1894 event has an estimated discharge of 17,000 m^3/s (Northwest Hydraulic Consultants 2008). The time series of systematic and historical discharge is given in Figure 2.1. The historical annual maximum discharge data used in the historical analysis is provided in Appendix B, Table B1.

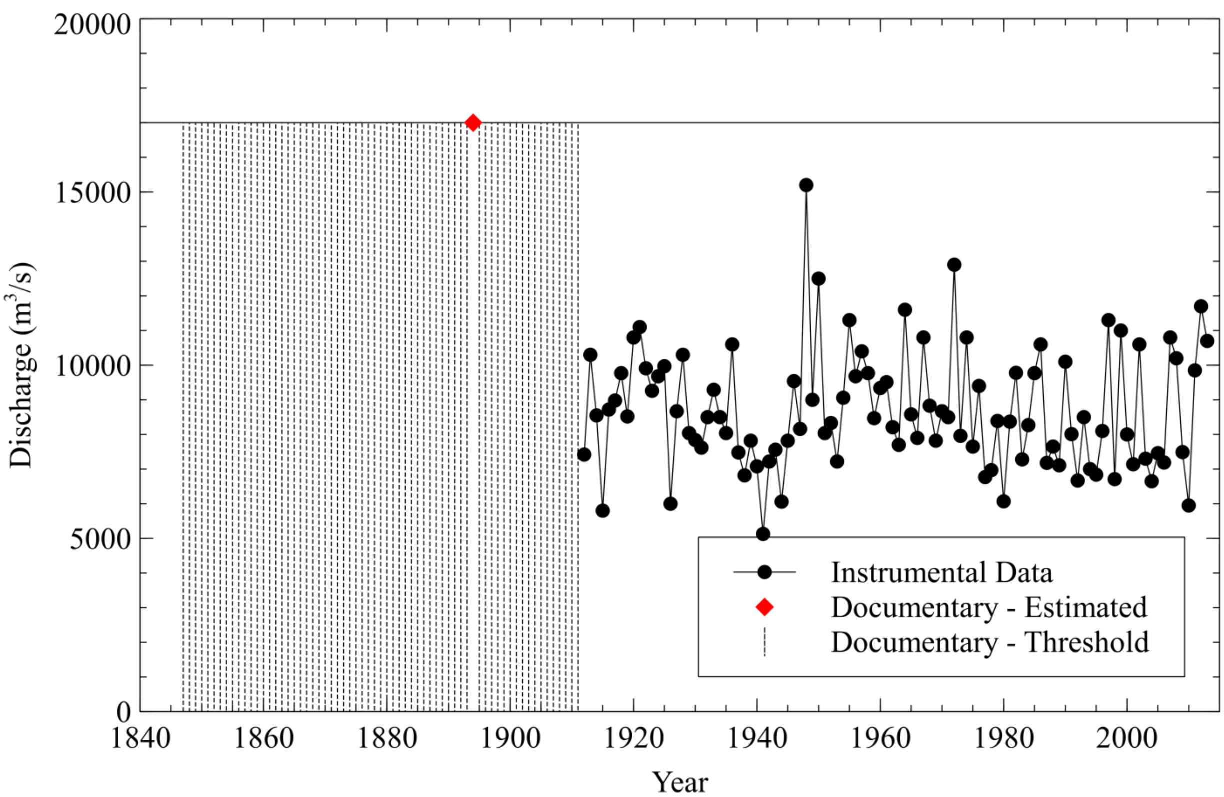

Figure 2.1. Time series of annual maximum peak discharge for the Fraser River at Hope, showing both instrumental and documentary discharge values.

2.2.1 *Stationary GEV Parameter Estimation*

Initial parameter estimation made use of the complete set of instrumental and documentary data in order to maintain consistency with previous work (Northwest Hydraulic Consultants 2008). For this initial approach we used Maximum likelihood (ML) estimation, an efficient and flexible approach which can easily incorporate all manner of historic information (Stedinger et al. 1993; Payrastre et al. 2011). We explored GEV parameter estimation using three different target data sets:

1) combined instrumental and documentary data (n=167);
2) only instrumental data (n=102); and
3) instrumental data, but including the 1894 event as an additional observation (n=103).

2.2.2 *Plotting Positions*

Probability plotting positions are used for the graphical display of flood peaks and as an empirical estimate of the probability of exceedance. In order to estimate the exceedance probability of annual maximum flood discharges comprised of both instrumental records as well as documentary records, we use the plotting positions suggested by Hirsch and Stedinger (1987). Following the nomenclature of Hirsch and Stedinger (1987), let n be the length (in years) of the historical period over which a set of flood events can be ranked, let s be the length of the systematic record period and let g consist of the complete record of observed floods where n>g>s. Among these floods there is a subset of "extraordinary" floods which are known to have ranks 1 through k over the period of length n, and let e be the number of extraordinary floods from the 1912-2013 record, where $e \leq k$ and $g = s + k - e$. Plotting positions have been calculated as:

$$\hat{p}_i = \begin{cases} p_e \dfrac{i-\alpha}{k+1-2\alpha} & i = 1, \dots, k \\ p_e + (1-p_e)\dfrac{i-k-a}{s-e+1-2a} & i = k+1, \dots, g \end{cases} \tag{5}$$

where $\hat{p}_i$ is the estimated exceedance probability, p_e is the probability of exceedance above the threshold y_T, estimated as k/n.

2.3 Nonstationary Analysis of Future Extreme Discharge

Presently (March 2015), streamflow projections based on the CMIP5 GCMs are unavailable. Given the computational cost and time required for downscaling GCMs and hydrologic modelling, a computationally efficient Generalized Extreme Value conditional density network (GEVcdn) model proposed by Cannon (2010, 2011) was employed. The model was developed and trained with inputs derived from the CMIP3 generation of GCMs and targets obtained from the corresponding VIC simulated peak streamflows (Shrestha et al. 2012). The model was then used to derive the discharge quantiles for the CMIP5 generation of the GCMs.

2.3.1 Nonstationary GEV Parameter Estimation

The "GEVcdn" R package (Cannon 2014) was employed for the evaluation of the GEV parameters. The GEVcdn is a probabilistic extension of the multilayer perceptron neural network, which expresses the GEV parameters as nonlinear function of covariates. Due to its nonlinear architecture, the model is capable of representing a wide range of nonstationary relationships, including interactions between covariates.

The GEVcdn structure consists of a three-layer interconnected network model (Cannon 2010), with the first (input) layer providing connections to the covariates, the second (hidden) layer providing connections to all inputs in the first layer, and the third (output) layer providing outputs in the form GEV parameters (Figure 2.2). Given covariates at time t, $x(t) = \{x_i(t), i = 1{:}I\}$, the output from the *j*th hidden layer node $\mathrm{h}_j(t)$ is given by transforming the signals using an activation function $f(.)$:

$$\mathrm{h}_j(t) = f\left(\sum_{i=1}^{I} w_{ji}{}^{(n)} x_i(t) + b_j{}^{(n)}\right) \tag{6}$$

Where, $w_{ji}{}^{(n)}$ is a hidden layer weight and $b_j{}^{(n)}$is a bias at node $n = 1{:}N$. The activation function $f(.)$ is taken to be the sigmoidal function $1/(1 + e^{-(.)})$ or hyperbolic tangent function $\tanh(.)$ for the nonlinear GEVcdn network and identity function for the strictly linear GEVcdn network. Similarly, the value at an output layer node $O_k(t)$ $(m = 1{:}3)$ is obtained as:

$$O_k(t) = f\left(\sum_{j=1}^{J} w_{kj}{}^{(m)} h_j(t) + b_k{}^{(m)}\right) \tag{7}$$

The output layer activation functions depend on the GEV parameter: identity for μ, $\exp(.)$ for σ (to ensure positivity), and $0.5 * \tanh(.)$ for ξ (to ensure values between -0.5 to 0.5):

The GEVcdn model parameters were estimated by using the ML approach (described in section 2.2.1) with the quasi-Newton algorithm used for optimization. The appropriate GEVcdn model hyper-parameters (i.e., number of hidden nodes and activation function) for a given dataset was selected by fitting models with different hyper-parameters and choosing the one that minimizes the Akaike information criterion with small sample size correction (AICc) (Akaike 1974; Hurvich and Tsai 1989). The AICc chooses the most parsimonious model that is capable of accounting for the true (but unknown) deterministic function responsible for generating the observations, thus, avoiding overfitting (fits the data to the noise rather than underlying signal) (Cannon 2010). Additionally, a part of the available data was kept aside (spilt-sampling) for an independent validation of the results.

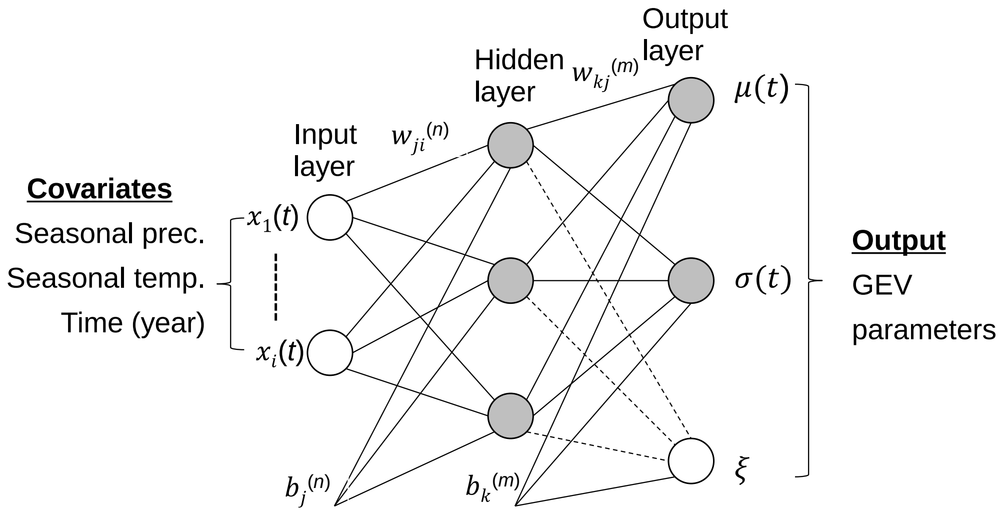

Figure 2.2. Structure of the GEVcdn model (adapted from Cannon 2010). The dashed lines connecting output node $\boldsymbol{\xi}$ show inactive connections when $\boldsymbol{\xi}$ is considered constant.

2.3.2 Covariates Evaluation

The first step in developing the GEVcdn model is selection of appropriate combination of covariates. In this study, this was determined in terms of the quantile verification score (QVS) (Friederichs and Hense 2007, 2008). The QVS is designed to assess the ability of a model to predict a certain quantile τ of a distribution. It is based on the asymmetrically weighted absolute deviation "check function" ρ_τ :

$$\rho_\tau(\epsilon) = \begin{cases} \epsilon\tau, & \geq 0 \\ \epsilon(\tau - 1), & \epsilon < 0 \end{cases} \tag{8}$$

where, ϵ is the difference between observations x_i and estimated quantiles $z_{\tau,i}(i = 1{:}N)$. The QVS for a given quantile τ is calculated as:

$$\mathrm{QVS}_\tau = \frac{1}{N}\sum_{i=1}^{N} \rho_\tau\,(x_i - z_{\tau,i}) \tag{9}$$

The QVS_τ is commonly expressed as a skill score with respect to a reference $\mathrm{QVS}_\tau(\mathrm{ref})$, which is expressed as.

$$\mathrm{QVSS}_\tau = 1 - \frac{\mathrm{QVS}_\tau}{\mathrm{QVS}_\tau(\mathrm{ref})} \tag{10}$$

QVSS_τ values lie between $-\infty$ and +1; positive values indicate that the model performance is better than the reference, and negative values mean that model performance is worse than the reference. In this case, the GEVcdn model skill is evaluated with reference to a stationary GEV model.

2.3.3 Model Implementation and Selection

The GEVcdn model was setup to emulate the statistical characteristics of the CMIP3 GCM driven VIC simulated peak discharges. The covariates were selected based on the physical factors driving peak discharge generation. Specifically, since peak discharge in spring is driven by winter/spring snow accumulation and melt, which in turn is driven by winter/spring temperature and precipitation, seasonal precipitation and temperature were taken as covariates. Additionally, as it is a common practice in nonstationary GEV analysis (e.g., Kharin and Zwiers 2005) time (year) is also considered as a covariate. The GEVcdn model was setup for four different combinations of covariates [(i) winter and spring precipitation, and spring temperature (djf P, mam P, mam T); (ii) winter and spring precipitation, spring temperature and year (djf P, mam P, mam T, Y); (iii) winter and spring precipitation, and winter and spring temperature (djf P, mam P, djf T, mam T); (iv) winter and spring precipitation, winter and spring temperature and time (djf P, mam P, djf T, mam T, Y)]. The model was trained by using the VIC simulated annual peak streamflows for corresponding GCMs as a target, and the network structure consisted of a single hidden layer and the number of neurons in the hidden layer varying from 1-10.

For the independent validation of the model results, the available data was divided into training and validation sets (spilt-sampling). Given that the VIC simulated streamflow peaks are similar for the CMIP3 A1B and A2 scenarios, the A1B and A2 datasets were separated into training and validation datasets, respectively. Additionally, the moderate B1 scenario data was used for training. Hence, the training dataset consisted of a pool of 15 GCMs x 138 years (1961-2098) from A1B (8 GCMs) and B1 (7 GCMs) scenarios, and the validation dataset consisted of a pool of 8 GCMs x 138 years (1961-2098) from the A2 emissions scenario. It is important to note that the CMIP3 driven results were primarily used for training the GEVcdn model. Given that only a few ensemble members are used, the CMIP3 results likely underestimate the total GCM uncertainty. Appendix B, Table B2 summarizes the GCMs and runs used to construct the CMIP3 climate projection ensemble.

Given that varying the shape parameter can result in three different types of GEV distribution (section 2.1) and hence make the distribution unstable, it is a common practice to assume the shape parameter to be constant (e.g. Cannon 2010; Katz 2013). In cases where the peak discharge regime changes (e.g., from nival to purely pluvial) it may be necessary to vary the shape parameter. In the case of Fraser River, such drastic changes were not projected to occur (Shrestha et al. 2012), and the shape parameter was assumed to remain constant. Hence, nonstationarity is represented by varying only the location and scale parameters. The best performing GEVcdn model was chosen using a two-step process. First, the number of hidden neurons in the network was selected based on the AICc performance criteria for each combination of covariates. Then, based on the comparison of the QVSS performance, the model with the overall best QVSS was selected.

Based on the covariates, GEVcdn produces a time series of the location, scale and shape parameters of the GEV distribution. The discharge quantiles obtained from the parameter time series depends on the covariates, which can be highly variable from year-to-year (e.g., Vasiliades et al. 2014). Such variability is mainly driven by the year-to-year differences in the covariates and their interactions. Additionally, part of the variable response could be attributed to natural climate variability. While such variability is useful for considering the likely range of discharge quantiles due to non-stationarity, the results become difficult to interpret for decision making and adaptation studies. Given that the scope of this project is to estimate the peak flow quantiles for select future 30-year periods we adopt a procedure that filters out the inter-annual variability and focuses on the underlying climate change signal. The procedure treats each 30-year period as stationary and employs resampling of the GEVcdn model results as follows:

1. For a 30-year period for each GCM, 5000 random realizations of exceedance probability p varying between 0 and 1 ($p = 0{:}\,1$) were used to calculate the discharge quantiles for each of the 30 sets of GEV parameters.
2. Using the 5000 realizations x 30-years, a stationary GEV distribution was fit for each GCM.
3. Using the fitted stationary models for the GCMs, discharge quantiles were calculated for the historical (1961-1990) and three future periods (2011-2040, 2041-2070, 2071-2098).

Based on the 30-year stationary GEV models for each GCM, future changes in the discharge quantiles for the CMIP3 and CMIP5 generation of GCMs were calculated using a two-step process:

1. The percentage change (scaling factor) in the discharge quantiles for each GCM for the three future periods was calculated relative to the historical period (1961-1990).
2. The future discharge quantiles were calculated by adjusting the historical discharge quantiles (section 2.2) with the scaling factors (delta method).

Covariates for the CMIP5-based projections were derived from 29 separate GCMs. For several of these GCMs, multiple runs[3] per emissions scenarios were also available for a total ensemble size of 46, 56 and 56 for the Representative Concentration Pathways (RCPs) 2.6, 4.5, and 8.5 emissions scenarios, respectively. Appendix B, Table B3 summarizes the CMIP5 GCM ensemble used in the current work.

[3] In the case of multiple runs (for a given emissions scenario), the same GCM is forced with slightly different initial conditions, which can result in a different climate trajectory for the same prescribed emissions. This process is conducted in order to sample internal variability of the climate system (i.e. variability due to processes within the climate system, as opposed to external variability, such as from anthropogenic activities)

3. RESULTS AND DISCUSSION

3.1 Stationary Historical Flood Frequency Analysis

Estimated quantile values were found to have little difference (not shown) based on parameters estimated using the three different data sets: 1) combined instrumental and documentary data (*n*=167); 2) only instrumental data (*n*=102); instrumental data, but treating the 1894 event as an additional observation (*n*=103). It is apparent that given the relatively long instrumental record for this site, the addition of documentary data has little overall effect on the quantile estimates. Fitting of the GEV distribution also reveals that the shape parameter is close to zero ($|\xi| < 0.01$), indicating that the GEV Type I distribution (Gumbel) is appropriate for modelling historical peak flow frequency. Further, as documentary data is not required, parameters can be estimated using the simpler method of L-moments (e.g. Stedinger et al. 1993), which provides very similar results to ML estimates. Hence, the historical peak flow frequency for the Fraser River at Hope is estimated by fitting the GEV Type I (Gumbel) distribution to the instrumental record augmented with the 1894 event (*n*=103) using the method of L-moments. The L-moment Gumbel estimates for the Fraser River at Hope are given in Table 3.1 and the empirical quantiles and the fitted Gumbel distribution is shown in Figures 3.1 and 3.2. Quantile estimates are also summarized in Table 3.2.

Approximate confidence intervals for both distribution parameters and quantiles are estimated by assuming that both parameters and quantiles are asymptotically normally distributed (Stedinger et al. 1993). The variance of the GEV Type I parameters and quantile variances are calculated from formulas provided by Phien (1987). Quantile uncertainty can be large, particularly at the higher return periods. For instance, the 1894 event has an estimated return period ~500 years (Figure 3.1 and Table 3.2), but the magnitude of a 500-year event has 5 to 95% confidence range of 16000 m^3/s to 18000 m^3/s (Figure 3.1). Likewise, the return period for an event of 17000 m^3/s magnitude ranges from 250 years to 1000 years (based on 5% to 95% confidence limits; Figure 3.2).

It is to be noted that the estimated long return period (1000-10000 years) quantile values are affected by a number of uncertainties, such as due to a limited number of sample points and changes in river geomorphological and watershed characteristics. Therefore, the long return period values presented in this and other sections of this report should be treated with a caution.

Table 3.1. L-moment Gumbel parameter estimates

Parameter	Parameter values		
	5th Percentile	Median	95th Percentile
μ	7744	7939	8134
σ	1293	1459	1625

Table 3.2. GEV Type I Distribution Quantile Estimates for the Fraser River at Hope

Return Period (Years)	Quantile Magnitude (m^3/s)		
	5th Percentile	Median	95th Percentile
10	10844	11222	11600
20	11787	12272	12757
50	13002	13632	14262
100	13909	14650	15392
200	14812	15665	16519
500	16001	17004	18007
1000	16900	18016	19132
2000	19027	17798	20257
5000	20364	18985	21744
10000	19882	21376	22869

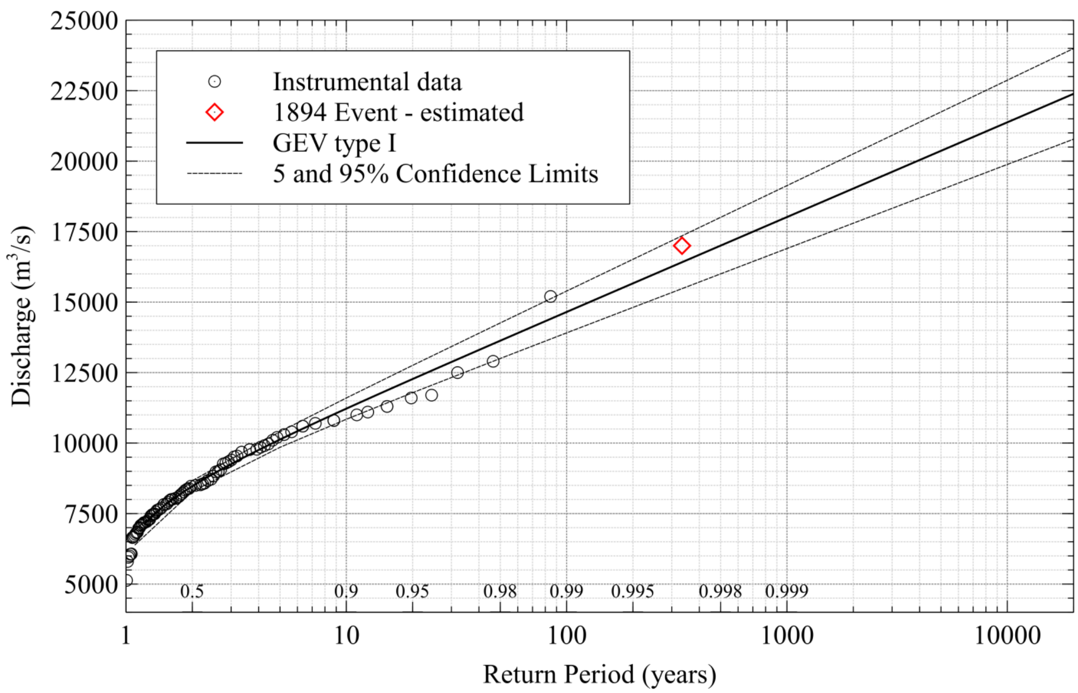

Figure 3.1. Plotting positions of observed and estimated historical events with fitted GEV Type I distributions showing discharge as a function of return period. Bottom axis shows the return period, as well as the non-exceedance probability.

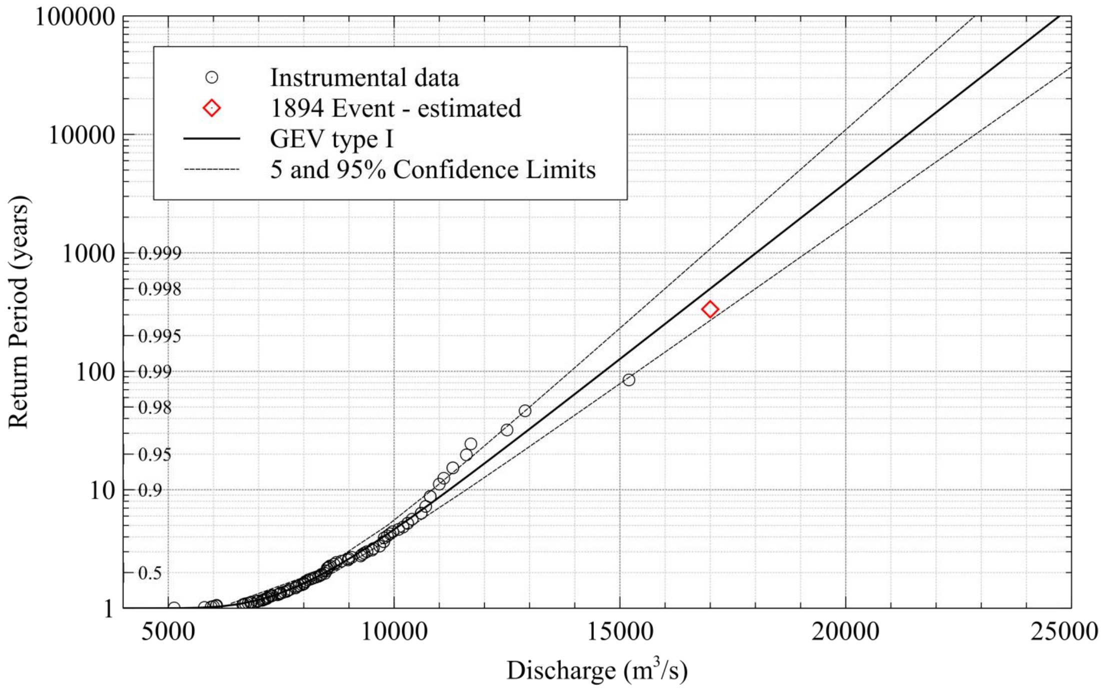

Figure 3.2. Plotting positions of observed and estimated historical events with fitted GEV Type I distributions showing return period as a function of discharge. Left axis shows the return period, as well as the non-exceedance probability.

3.2 Nonstationary Analysis of Future Extreme Discharge

3.2.1 Evaluation of Training and Validation Results

The Quantile Verification Skill Score (QVSS) for the training dataset using the four different combinations of covariates are shown in Figure 3.3a. In all cases, the stationary model was used as a reference. Relative to the reference model, all four nonstationary models showed positive skills ranging between 0.17 and 0.26. Comparing the results with and without time as a covariate, i.e., (i) vs. (ii), and (iii) vs. (iv), in both cases, the results show better QVSS scores when time is used as a covariate. Overall, the results for the training dataset showed a superior model performance for the model trained with winter and spring precipitation, winter and spring temperature and time (djf P, mam P, djf T, mam T, Y), except for 1000-year return period. Based on the results, model (iv) was selected as the best model for the evaluation of the CMIP3 and CMIP5 quantile discharges. Similar results were also obtained for the validation dataset (Figure 3.3b), with the stationary GEV parameters obtained from the training dataset used as the reference model.

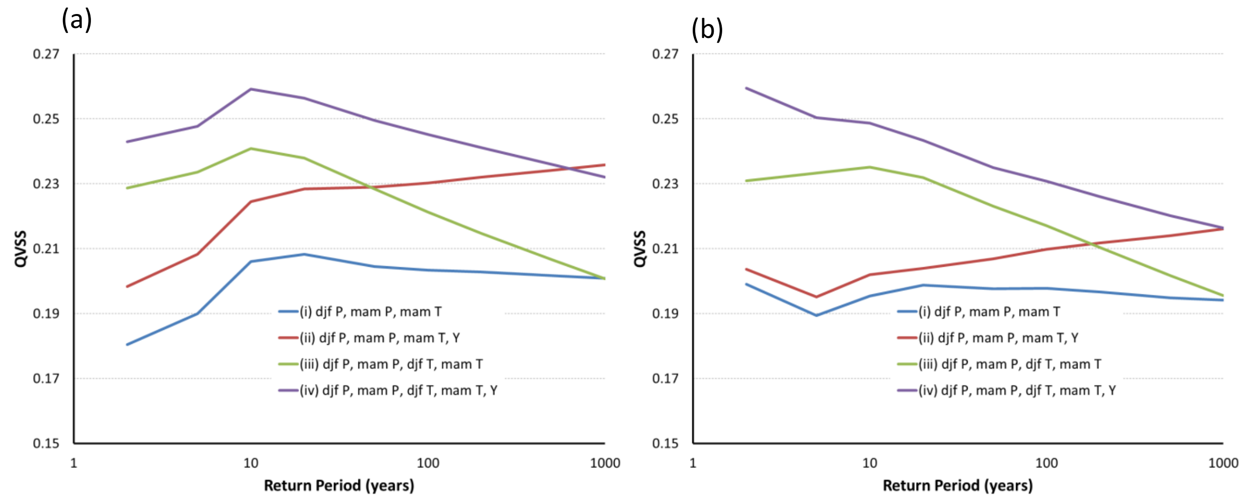

Figure 3.3. QVSS for (a) training and (b) validation datasets for four the combination of covariates: (i) winter and spring precipitation, and spring temperature (djf P, mam P, mam T); (ii) winter and spring precipitation, spring temperature and year (djf P, mam P, mam T, Y); (iii) winter and spring precipitation, winter and spring temperature (djf P, mam P, djf T, mam T); (iv) winter and spring precipitation, winter and spring temperature and time (djf P, mam P, djf T, mam T, Y).

Table 3.3. Range of GEV parameters obtained from the GEVcdn model (iv)

Parameter	Values (minimum, median, maximum)	
	Training	**Validation**
μ	4792, 7984, 13103	5586, 7901, 12742
σ	333, 1184, 2395	630, 1196, 2875
ξ	-0.101	-0.101

Table 3.3 shows the range of GEV parameters obtained for the calibration and validation datasets. The ξ parameter was assumed constant, and its negative value means that the distribution is bounded or Weibull type.

In order the test the ability of the model to simulate the quantiles of annual maximum discharge, random realizations of exceedance probability p varying between 0 and 1 ($p = 0{:}\,1$) were sampled to calculate the discharge quantiles for a set of 98 (for 2001-2098 period) GEV parameters for each GCM. The discharge quantiles obtained for 15 GCM (training) and 8 GCMs (validation) were compared with the VIC model flow quantiles for the corresponding datasets. The quantile-quantile plots in Figure 3.4 show that, except for some discrepancies at the maximum values, the quantile-quantile values are close to the one-to-one relationship line, both for the training and validation datasets. This illustrates a good ability of the model to simulate the discharge quantiles.

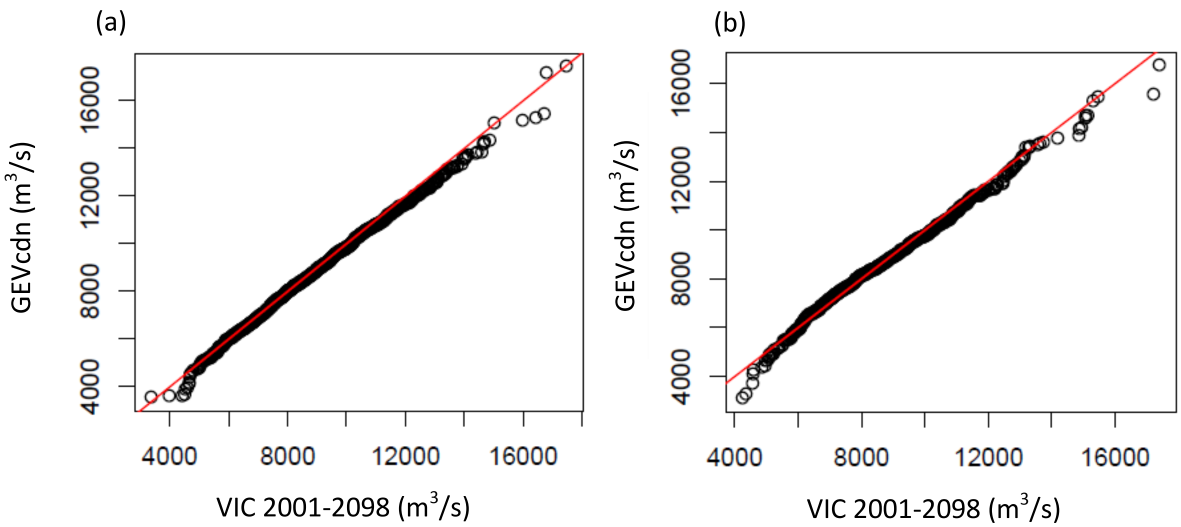

Figure 3.4. Quantile-quantile plots of VIC simulated results and a random realization GEVcdn model for (a) training and (b) validation datasets. The red line shows the one-to-one relationship.

Figure 3.5 further illustrates the ability of the GEVcdn model to represent the variability of the VIC simulated streamflow peaks. The GEVcdn model captures the general temporal patterns in the VIC results with a wider spread between the 95th and 5th percentiles as we move into the end of 21st century. The results, however, also illustrate high inter-annual variability. Thus, for the evaluation of the climate driven changes in streamflow extremes, we filter out the inter-annual variability by considering peak flow change in the context of stationary 30-year periods.

3.2.2 Future Changes in Discharge Quantiles for CMIP3 GCMs

Streamflow extremes in the Fraser River occur as a result of winter and spring precipitation and temperature and their interactions with snow storage. Specifically, higher precipitation leads to larger snowpack, while higher temperature leads to earlier depletion of the snowpack and a greater proportion of precipitation occurring as rainfall. Such interactions for each of the GCM ensemble members are expected to affect the future frequency and magnitude of streamflow extremes. For illustration, the future December-May temperature (°C) and precipitation (%) changes relative to the historical period (1961-1990) are summarized in Table 3.4. In general for all three scenarios, both precipitation and temperature are projected to increase in the future, with a progressively higher increase for the three future.

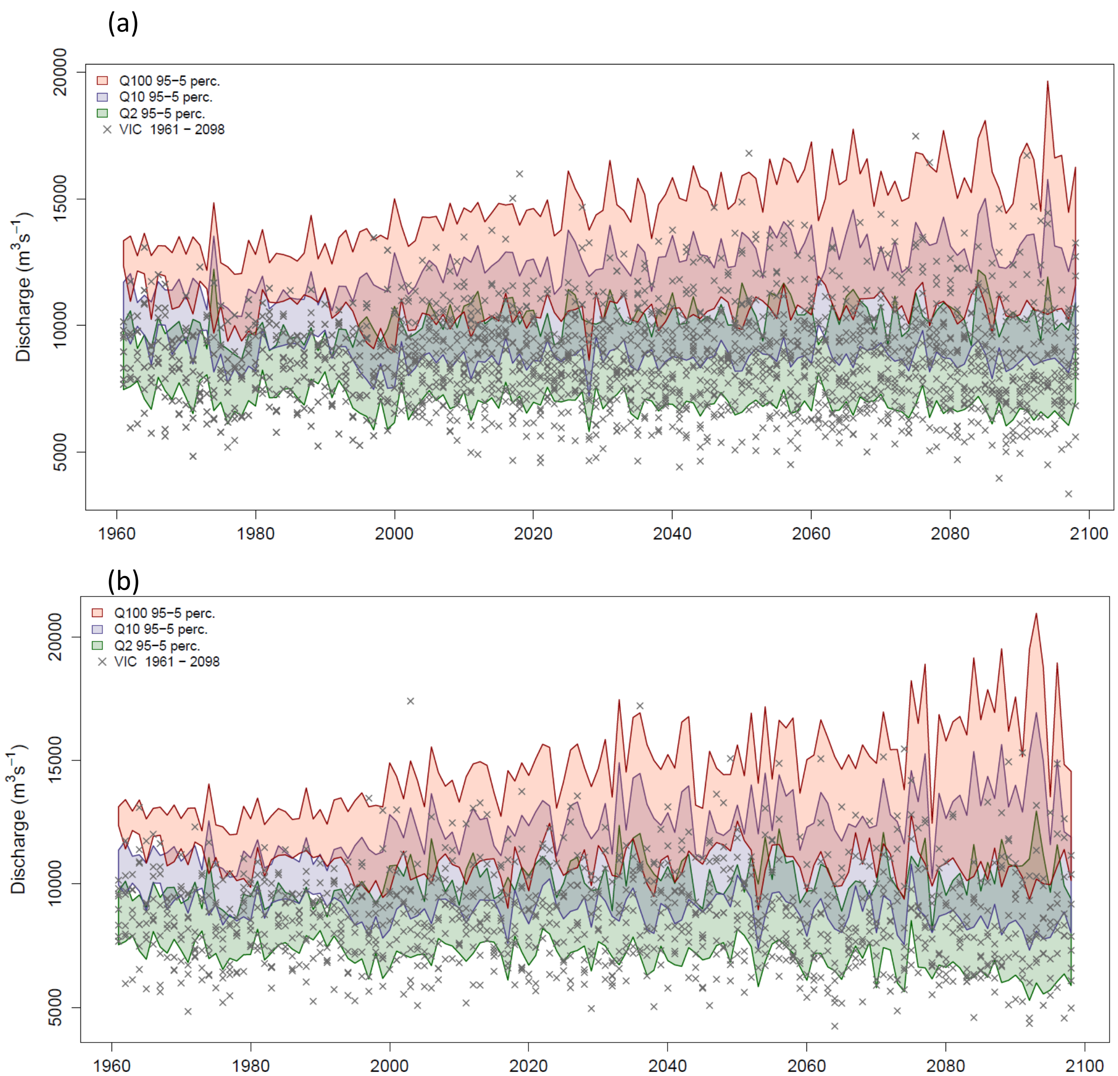

Figure 3.5. 95th and 5th percentiles envelopes from the GEVcdn model obtained from CMIP3-based GCM ensembles for the 2-year, 10-year and 100-year return period discharges for (a) training and (b) validation datasets. The grey crosses represent the VIC simulated peak flows for the corresponding GCMs. Training is based on the B1 and A1B emissions scenarios, validation is based on the A2 scenario.

Using the procedure described in section 2.3.3, we fitted stationary GEV distributions for each of the 30-year (1961-1990, 2011-2040, 2041-2070) and 28-year (2071-2098) periods and calculated quantile discharges for each respective period. Based on these discharge quantiles, we calculated the percentage change for the three future periods (2011-2040, 2041-2070, 2071-2098) relative to the historical period (1961-1990). Table 3.5 shows the minimum, median and maximum values obtained from the GCM ensembles. Results from all GCMs are summarized in Appendix B, Table B4.

Table 3.4. Changes in the 30-year mean (28-year for 2071-2098) future December-May temperature (°C) and precipitation (%) relative to the historical period (1961-1990). The minimum, median and maximum values are obtained for the CHIP3 GCM ensembles.

Scenario	Future period		Temperature change (°C)	Precipitation change (%)
B1	2011-2040	Min.	0.7	-3
		Med	1.3	6
		Max	2.1	8
	2041-2070	Min.	1.0	7
		Med.	1.9	12
		Max	3.3	15
	2071-2098	Min.	1.6	4
		Med.	2.7	13
		Max.	4.5	21
A1B	2011-2040	Min.	0.8	4
		Med	1.5	7
		Max	1.9	10
	2041-2070	Min.	1.8	7
		Med.	2.6	12
		Max	3.2	21
	2071-2098	Min.	2.5	10
		Med.	3.5	15
		Max.	4.7	27
A2	2011-2040	Min.	0.3	0
		Med	1.4	7
		Max	1.8	10
	2041-2070	Min.	1.0	2
		Med.	2.3	8
		Max	2.8	17
	2071-2098	Min.	2.6	9
		Med.	4.1	20
		Max.	5.0	38

While the results for the three scenarios are similar for 2041-2070, they diverge for 2071-2098 with the smallest increase for the B1 scenario and the largest increase for the A2 scenario. Specifically, the median increases in 2071-2098 for the ensembles are 9% to 24%, 7% to 20% and 8% to 39% (range are for 10 year-10000 year return periods) for B1, A1B and A2 scenarios, respectively. The maximum increases in 2071-2098 are 14% to 41%, 15% to 52% and 25% to 75% for B1, A1B and A2 scenarios, respectively.

The combination of increasing temperature with increasing precipitation tends to result in reduced snow accumulation and increased rainfall. On a seasonal basis these climate changes are anticipated to result in increased winter discharge, an earlier spring freshet, and reduced summer discharge (Shrestha et al. 2012; Schnorbus et al. 2014). We posit that the modelled increase in peak annual maximum discharge, despite decreasing snow accumulation, results from some combination of increased melt rates (for the snow that remains) and more frequent rainfall occurrence during the freshet period.

Based on the percentage change in the quantile discharges, future discharge quantiles were calculated by adjusting the discharge quantiles obtained from the Gumbel distribution for the historic data (Table 3.1). The results for all GCMs are summarized in Appendix B, Table B5. Figure 3.6 (a, b, c) depicts the historical and adjusted flood frequency curves for the three future periods using the moderate A1B emissions scenario. The flood frequency curves for the B1 and A2 emissions scenarios are available in Appendix C, Figures C1 and C2, respectively. Although the resulting curves for some of the GCMs show decreases in quantile discharges, those for most GCMs show increases. Additionally, the larger quantiles (e.g., 5000-year and 10000-year return periods) tend to show a greater divergence from the historical values. However, these large qualities are subject to much higher uncertainty due to a sampling variability (i.e., only a limited number of data points available for fitting the GEV distribution).

Table 3.5. Percentage change in discharge quantiles for the three future periods relative to the historical period of 1961-1990. The minimum, median and maximum values are obtained from the CHIP3 GCM ensembles.

Scenario	**Future period**		**% change in quantile discharge for return periods**								
			10	**50**	**100**	**200**	**500**	**1000**	**2000**	**5000**	**10000**
B1	2011-2040	Min.	-2	1	2	3	4	5	6	7	8
		Med	4	6	7	8	8	9	9	10	10
		Max	10	12	13	14	15	16	17	18	20
	2041-2070	Min.	0	4	5	6	7	9	10	11	12
		Med.	9	14	16	18	21	22	23	25	25
		Max	14	19	20	22	24	25	27	29	30
	2071-2098	Min.	0	4	5	7	8	9	11	12	13
		Med.	9	15	17	19	20	21	22	23	24
		Max.	14	19	22	25	29	31	34	38	41
A1B	2011-2040	Min.	1	3	3	3	3	3	3	4	4
		Med	6	8	8	9	10	10	11	12	13
		Max	13	19	21	24	27	29	31	34	36
	2041-2070	Min.	-1	3	3	4	5	6	7	8	8
		Med.	6	9	10	12	14	16	18	20	22
		Max	17	22	23	24	27	28	31	34	37
	2071-2098	Min.	-3	0	1	3	4	5	6	7	8
		Med.	7	10	12	13	15	16	17	19	20
		Max.	15	24	28	31	36	40	44	48	52
A2	2011-2040	Min.	-1	2	4	4	4	4	4	4	4
		Med	6	11	14	16	19	20	22	23	24
		Max	12	18	20	23	26	28	31	34	36
	2041-2070	Min.	-3	0	2	3	5	6	7	8	9
		Med.	6	10	12	13	15	16	17	18	19
		Max	15	21	23	25	28	29	31	33	34
	2071-2098	Min.	-3	6	10	13	15	17	19	21	23
		Med.	8	18	21	24	27	30	32	35	39
		Max.	25	37	41	46	53	58	63	70	75

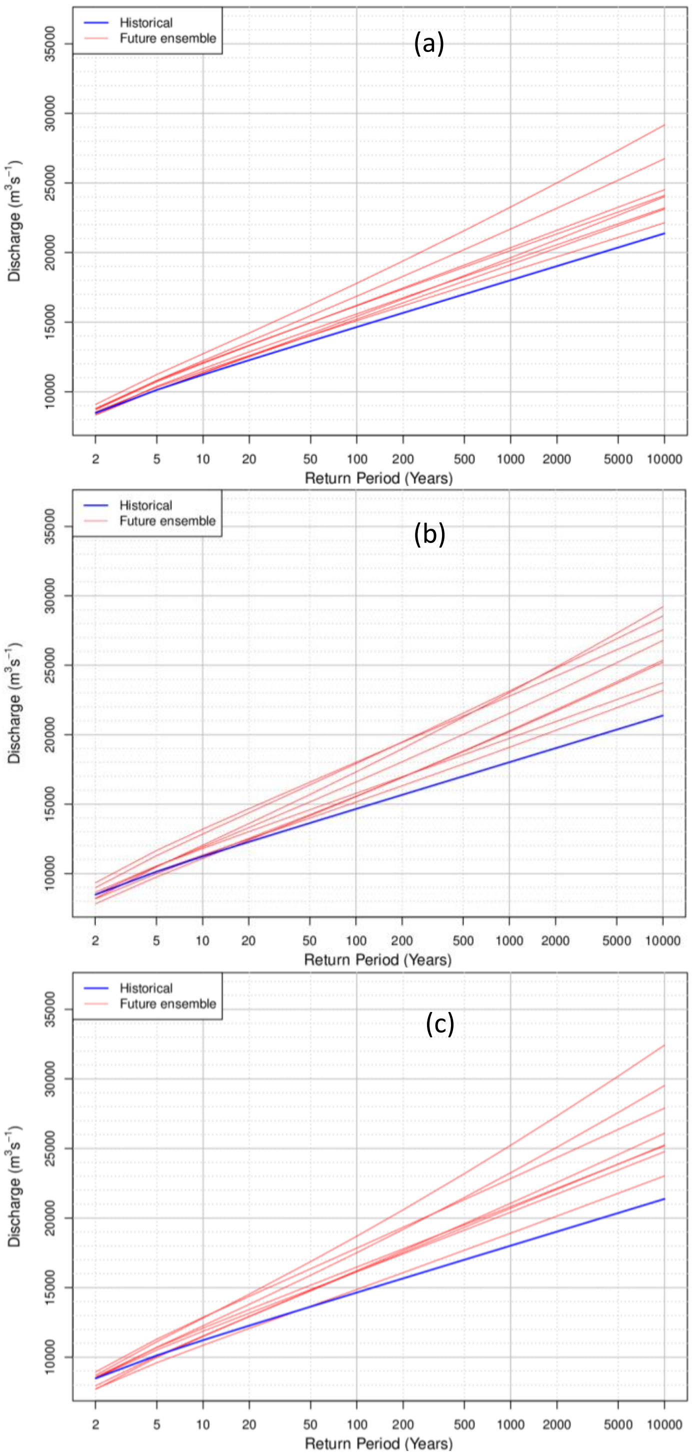

Figure 3.6. Future (CMIP3 A1B emissions scenario) flood frequency curves compared to the historical plot for the periods (a) 2011-2040; (b) 2041-2070; and (c) 2071-2098.

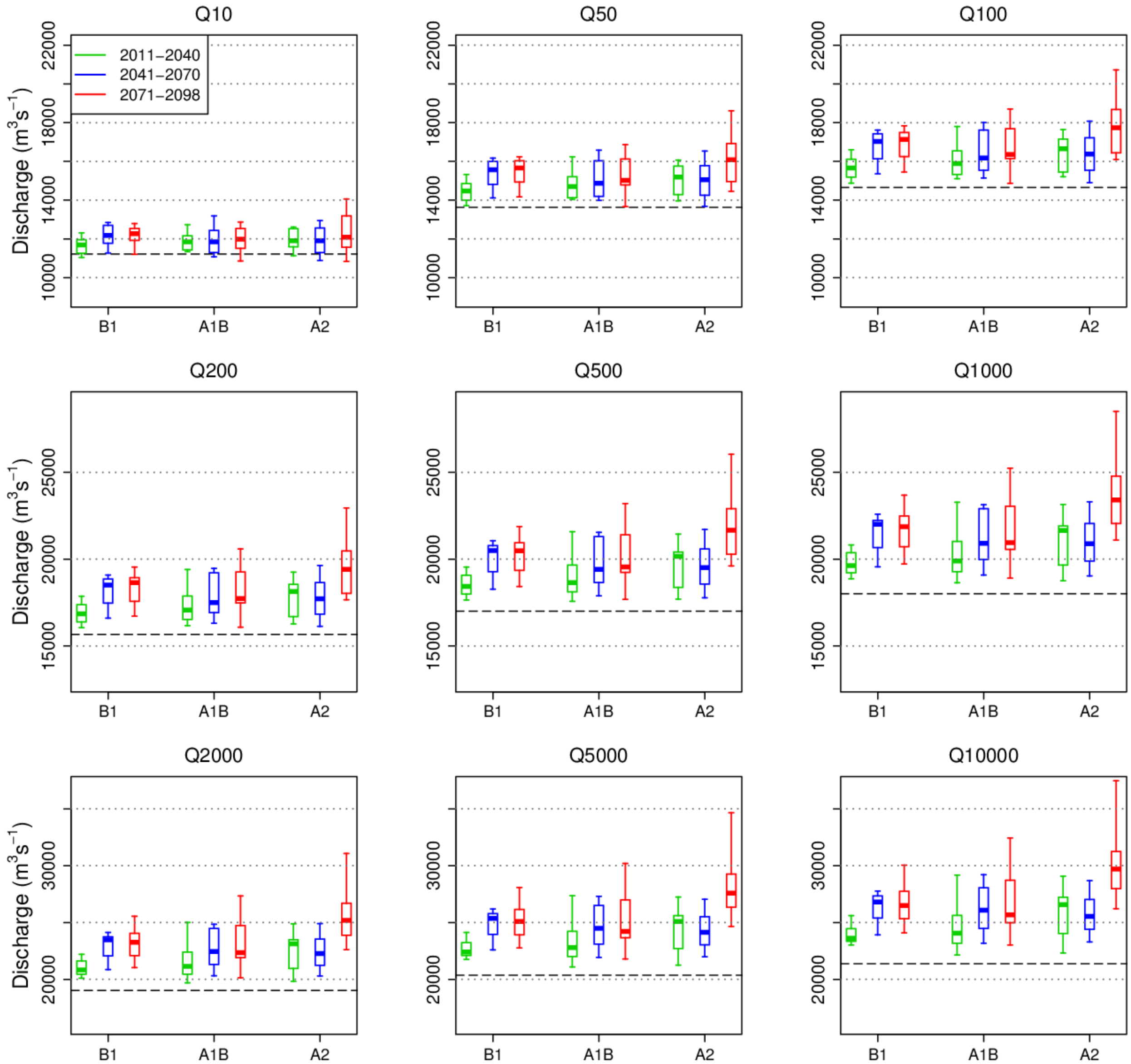

Figure 3.7. Box plots showing the change in the discharge quantiles for the three CMIP3 emissions scenarios compared to the historical period shown by the dashed line. Each box illustrates the median and inter-quartile range, and the whiskers show the upper and lower limits obtained from the GCM ensembles.

Figure 3.7 summarizes the change in discharge quantiles for the three emissions scenarios and the future periods compared to the historical period. This again illustrates the increase in future discharge values for all GCMs and return periods.

3.2.3 Future Changes in Discharge Quantiles for CMIP5 GCMs

Table 3.6 summarizes the mean future December-May temperature (°C) and precipitation (%) relative to the historical period (1961-1990). Given the larger number of CMIP5 GCM ensembles used (46, 56 and 56 GCMs for RCPs 2.6, 4.5, and 8.5, respectively), the results cover a larger range of GCM uncertainty and the spread between the minimum and maximum values are larger than the CMIP3 results (Table 3.4). For all three RCPs, both precipitation and temperature generally show progressive increases for the three future periods, with the smallest increases for RCP2.6 and the largest increases for RCP8.5. For all three RCPs, the spread between the ensemble members also tend to get progressively wider for the three future periods, due to larger GCM uncertainties.

Table 3.6. Changes in the 30-year mean future December-May temperature (°C) and precipitation (%) relative to the historical period (1961-1990). The minimum, median and maximum values are obtained for the CHIP5 GCM ensembles.

Scenario	Future period		Temperature change (°C)	Precipitation change (%)
RCP2.6	2011-2040	Min.	0.5	-5
		Med	1.6	8
		Max	3.1	20
	2041-2070	Min.	1.2	-4
		Med.	2.1	10
		Max	4.1	20
	2071-2100	Min.	1.1	-6
		Med.	2.4	10
		Max.	4.7	21
RCP4.5	2011-2040	Min.	0.5	-1
		Med	1.4	7
		Max	2.9	17
	2041-2070	Min.	1.2	-2
		Med.	2.6	11
		Max	4.6	27
	2071-2100	Min.	1.4	2
		Med.	3.3	12
		Max.	5.2	27
RCP8.5	2011-2040	Min.	0.7	-2
		Med	1.7	7
		Max	2.8	18
	2041-2070	Min.	1.9	-3
		Med.	3.3	13
		Max	5.4	35
	2071-2100	Min.	3.1	2
		Med.	5.5	20
		Max.	8.0	41

Using the same methodology described above for the CMIP3 GCMs, percentage changes in discharge quantiles were calculated. The minimum, median and maximum values obtained from the GCM ensembles are summarized in Table 3.7 and all CMIP5 GCMs results are summarized in Appendix B, Table B6. Note that for those GCMs with multiple runs, results from only a single run (run 1) are given. The results generally show increases in discharge quantiles for all return periods, RCPs and future periods. Compared to CMIP3 (Table 3.5), the maximum-minimum ranges are also larger, mainly due to the larger number of ensemble members considered. RCP8.5 has the largest increase and widest range compared to RCP2.6 and RCP4.5. The range of median increases in 2071-2100 are 5% to 15%, 3% to 18% and -3% to 24% for RCP 2.6, 4.5 and 8.5, respectively. Maximum changes for 2071-2098 range from 15% to 53%, 21% to 52% and 22% to 74% for RCP 2.6, 4.5 and 8.5, respectively.

Table 3.7. Percentage change in discharge quantiles for the three future periods relative to the historical period of 1961-1990. The minimum and maximum values are obtained for the CMIP5 GCM ensembles.

Scenario	**Future period**		**% change in quantile discharge for return periods**								
			10	**50**	**100**	**200**	**500**	**1000**	**2000**	**5000**	**10000**
RCP2.6	2011-2040	Min.	-10	-10	-9	-9	-8	-7	-8	-9	-10
		Med	2	4	6	7	8	9	9	10	11
		Max	9	14	17	20	26	30	35	42	47
	2041-2070	Min.	-5	-4	-4	-4	-4	-5	-5	-5	-5
		Med.	5	10	11	12	15	16	17	17	18
		Max	18	28	32	37	42	47	53	62	68
	2071-2100	Min.	-5	-4	-4	-5	-6	-7	-8	-9	-10
		Med.	5	8	10	11	11	13	14	14	15
		Max.	15	20	23	28	33	38	42	49	53
RCP4.5	2011-2040	Min.	-10	-8	-8	-9	-9	-9	-9	-9	-9
		Med	3	5	6	7	8	9	9	10	11
		Max	11	14	16	18	21	23	26	29	31
	2041-2070	Min.	-8	-7	-7	-7	-8	-8	-8	-9	-9
		Med.	2	5	6	8	10	11	12	14	15
		Max	22	25	25	27	31	34	37	41	44
	2071-2100	Min.	-7	-6	-5	-5	-5	-6	-6	-7	-7
		Med.	3	7	9	10	12	14	15	17	18
		Max.	21	28	31	34	38	41	44	48	52
RCP8.5	2011-2040	Min.	-10	-10	-9	-10	-11	-12	-13	-14	-15
		Med	0	3	4	5	7	8	9	10	11
		Max	13	21	24	27	31	35	38	42	45
	2041-2070	Min.	-13	-12	-12	-12	-13	-13	-14	-14	-15
		Med.	-2	3	5	6	8	10	12	13	15
		Max	20	25	27	31	36	39	43	47	52
	2071-2100	Min.	-20	-19	-19	-19	-19	-19	-19	-20	-20
		Med.	-3	6	9	12	15	17	19	22	24
		Max.	22	34	39	44	51	56	61	68	74

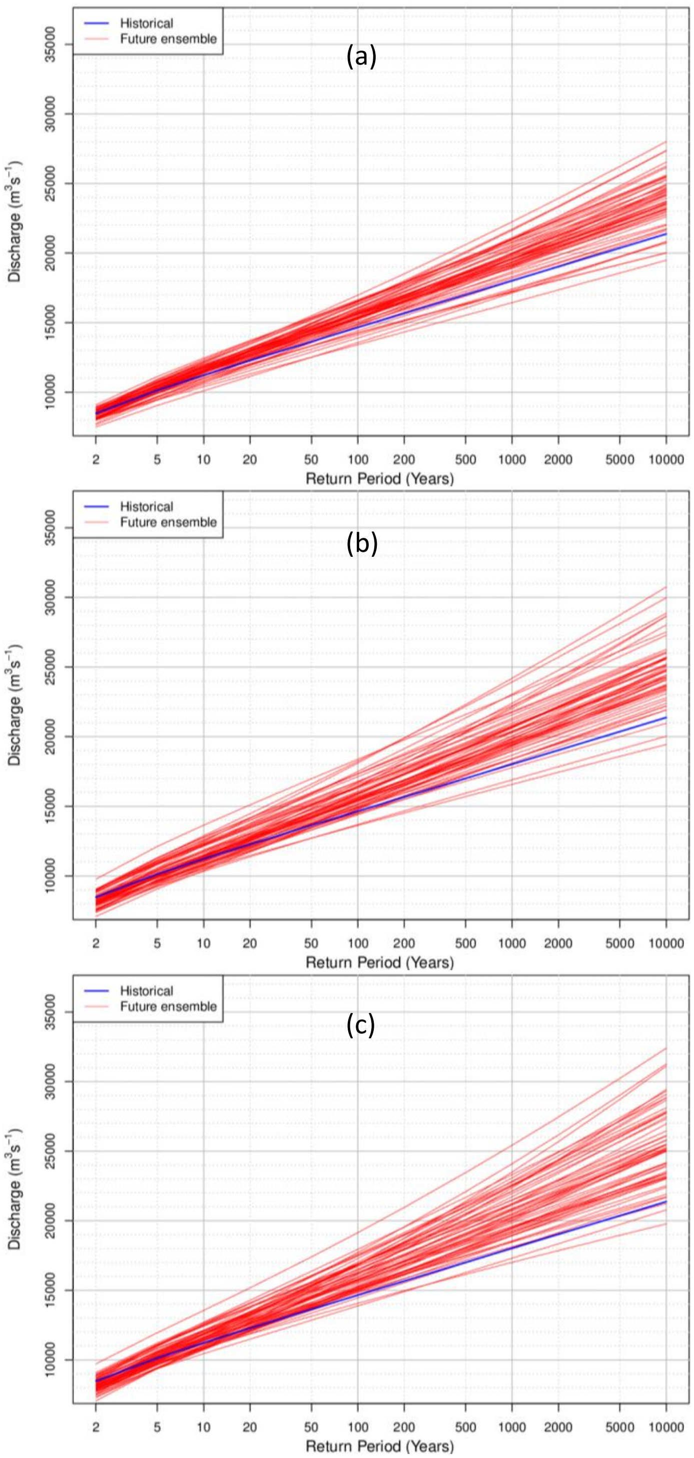

Figure 3.8. Future (CMIP5, RCP4.5) flood frequency curves compared to the historical plot for the periods (a) 2011-2040; (b) 2041-2070; and (c) 2071-2100.

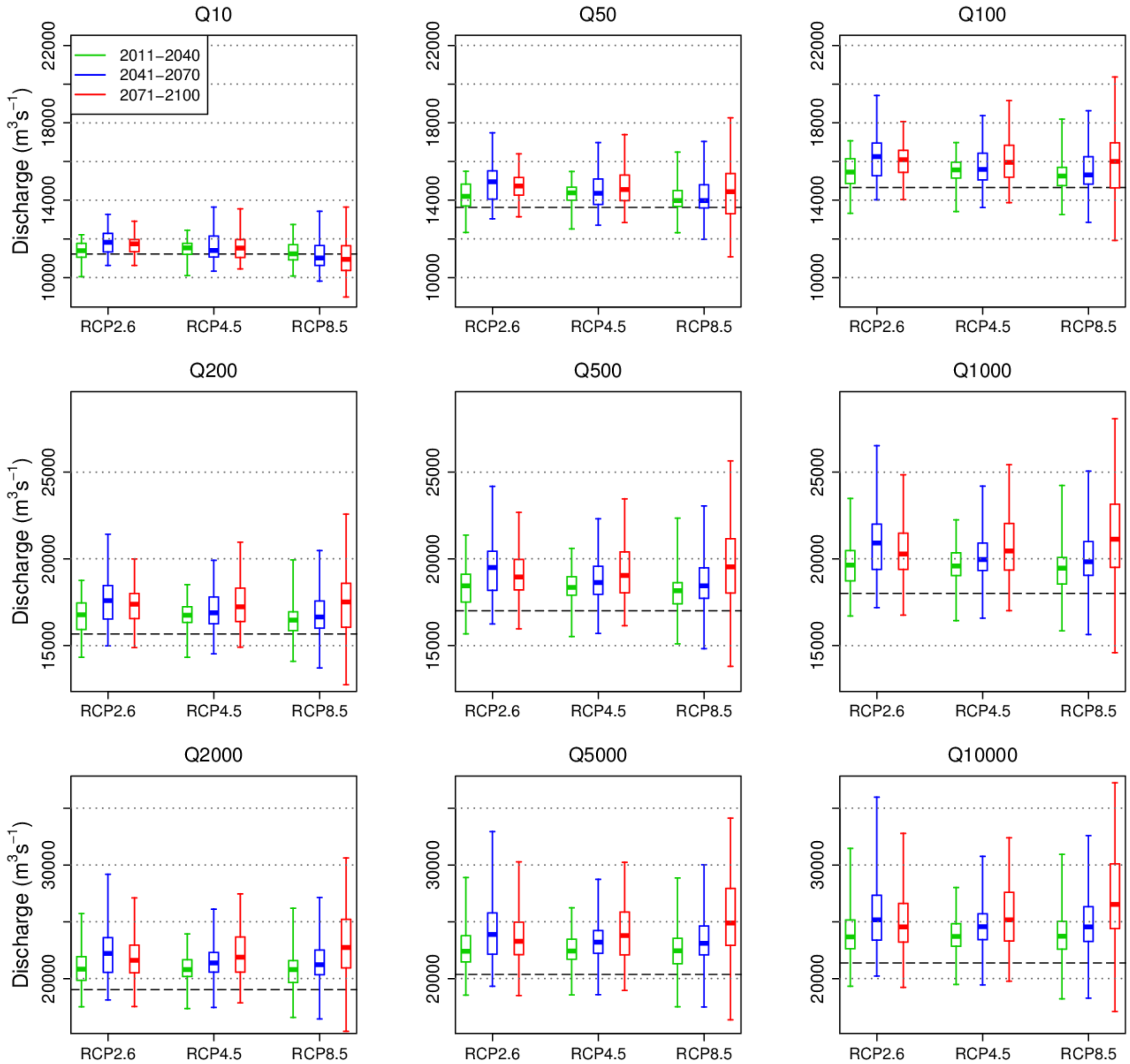

Figure 3.9. Box plots showing the change in the discharge quantiles for the three CMIP representative concentration pathways compared to the historical period shown by the dashed line. Each box illustrates the median and inter-quartile range, and the whiskers show the upper and lower limits obtained from the GCM ensembles.

The future discharge quantiles, calculated by adjusting the historical discharge quantiles (Figure 3.1; Table 3.1) with the percentage changes, are summarized in Appendix B, Table B7. Note that for those GCMs with multiple runs, results from only a single run (run 1) are given. The flood frequency curves for the moderate RCP (RCP4.5) are shown in Figure 3.8 (a, b, c), which depict a wider range compared to the CMIP3 A1B results (Figure 3.6a, b, c), attributable to wider range of precipitation and temperature projections for the CMIP5 GCMs. In this case also, the spread of the discharge quantiles tends to increase with increasing return periods. Additionally, the ensemble spread tends to get progressively wider for 2011-2040, 2041-2070 and 2071-2100. The frequency curves for the RCP2.6 and RCP8.5 are available in Appendix C, Figures C3 and C4, respectively.

Figure 3.9 summarizes the future discharge quantiles for the three RCPs compared to the historical period. The results depict a tendency for increased quantile discharges in the future. Specifically, although several individual projections indicate decreased quantile values, the ensemble median values generally show progressively increasing quantile values for the three future periods for all return periods (excepting *T*=10 years). An exception to this is RCP2.6 scenario, which shows the quantile values peaking in mid-century (2014-2070), which is a consequence of the emissions for this RCP also peaking in mid-century (see Appendix A for a description of emissions scenarios).

3.2.4 Uncertainties in Estimating Discharge Quantiles

Uncertainty is an inherent in the development of hydrologic projections. The quantification of projected changes in annual maximum peak flow quantiles based on the methodology employed is affected by the following main sources of uncertainty:

1. Choice of emissions scenario;
2. GCM structure;
3. Climate variability;
4. Hydrologic model and GEVcdn model structure; and
5. Sampling variability.

Climate projections are affected by uncertainties arising from the unknown trajectory of future greenhouse gas (GHG) emissions, GCM model structure, natural variability of the climate system, and choice of downscaling method (Kay et al. 2008). Previous studies (Kay et al. 2008; Prudhomme and Davies 2008a,b; Bennett et al. 2012) indicated that, in the context of hydrologic projections, GCM structure is the largest source of uncertainty. The climate's natural chaotic internal variability, which is represented by ensemble members of a climate model, can also have appreciable impacts on the sensitivity of some of the outputs (Kendon et al. 2010; Deser et al. 2012). For the CMIP5-based projections the uncertainties related to the GHG emissions, GCM structure and natural climate variability have been explicitly taken into account by using a large ensemble of different GCMs with multiple runs (for select GCMs) for a range of emissions scenarios. It is to be noted that the CMIP3-based projections use a much more limited number of GCMs, with only a single run from each model (ensemble size of 7, 8 and 8 for B1, A1B and A2, respectively). Hence, projection uncertainty is likely underestimated for the CMIP3 results. Nevertheless, this is not considered problematic as the CMIP3-based climate projections are primarily used for training and validation of the GEVcdn model. Uncertainty due to downscaling has not been explicitly addressed, but is expected to be a minor component of overall climate projection uncertainty.

The VIC model simulated CMIP3 streamflow used for setting up the GEVcdn model is also affected by uncertainties. Specifically, hydrologic models are affected by errors in input data, model structure, and parameter specification (Beven 2006). These errors affect the ability of a hydrologic model in replicating the observed variability of streamflow, including streamflow extremes (Shrestha et al. 2014). However, the use of a simple scaling approach to estimate future discharge quantiles (i.e. the 'observed' peak flow frequency is scaled according to quantile changes modelled using GEVcdn) is expected to mitigate the effect of any VIC model bias in simulating annual maximum peak flow. The application of the GEVcdn methodology for estimating future discharge is also subject to uncertainty. Firstly, the chosen covariates may not fully describe the mechanism for generation of annual maximum peak streamflows and, secondly, given the limited extrapolation capability of a neural network, the GEVcdn model is not suitable for estimating discharge quantiles beyond the range of training dataset. However, model verification (see Section 3.2.1) indicates that the GEVcdn model is accurate and robust and the CMIP5 climate projections are within the range of the CMIP3 training data. VIC- and GEVcdn-related errors and uncertainties are judged to be relatively minor with respect to the uncertainties in the climate projections.

Lastly, GEV parameter estimation (for both stationary and nonstationary parameters) is also affected by uncertainties due to sampling variability (Kharin and Zwiers 2005). In particular, the effect of sampling variability can be considerable for the longer return period flow quantiles (e.g., > 1000 years). As such we advise caution when using peak discharge values reported herein for such high return period (low probability) events.

4. CONCLUSIONS AND FUTURE WORK

This study evaluated potential future changes in flood frequencies for the Fraser River at Hope station (WSC gauge 08MF005). The analysis was conducted using the GEV conditional density network (GEVcdn) statistical model, which provides a flexible, efficient and robust means of estimating the nonstationary distribution of annual maximum streamflow events using the Generalized Extreme Value (GEV) distribution. Results are presented for a range of possible future emission scenarios spanning low, medium and high emission (e.g. CMIP3) or strong mitigation, stabilization or high emissions (i.e. business-as-usual; CMIP5) using output from a large pool of GCMs derived from two separate global climate modelling experiments. Although not explicitly predictions of the future, the provided projections cover wide and realistic range of possible future outcomes and, hence, will prove useful for flood management and adaptation activities.

In the first part of this work, a stationary analysis of extreme historical discharge was conducted based on 102-year (1912-2013) historical peak annual maximum daily flow data, supplemented with estimated 1894 peak discharge value. Based on the fitted Gumbel distribution, the 1894 event (≈ 17000 m^3/s) has a return period of about 500 years, with a 16000 m^3/s to 18000 m^3/s confidence range (5% to 95%). Alternatively, a 17000 m^3/s event is estimated to have a return period ranging from 250 to 1000 years (also based on 5% to 95% confidence range). .

In the second part of this study, a nonstationary analysis of the VIC model simulated historical/future discharge was conducted with the GEV parameters expressed as a function of covariates. The GEV conditional density network (GEVcdn) was employed for the estimation of GEV parameters, with covariates consisting of seasonal precipitation and temperature from CMIP3 and time (year). The results of the GEVcdn nonstationary model showed a good ability of the model to simulate quantile discharges and a reasonable representation of the temporal patterns in the VIC simulated streamflow extremes. The results also illustrate high inter-annual variability in the parameters of the GEV distribution. Thus, for the evaluation of the climate driven changes in streamflow extremes, we used 30-year climatological periods, which we treated as stationary, and evaluated future change in discharge quantiles relative to the discharge quantiles from a baseline historical period. Results of the analysis showed increases in flow quantiles for both the CMIP3- and CMIP5-based projections, with progressively larger increases for 2011-2040, 2041-2070 and 2071-2100. The median increases in 2071-2098 based on CMIP3 GCM ensembles are 9% to 24%, 7% to 20% and 8% to 39% (range are for 10 year-10000 year return periods) for B1, A1B and A2 scenarios, respectively. The maximum increases in 2071-2098 from CMIP3 GCM ensembles are 14% to 41%, 15% to 52% and 25% to 75% for B1, A1B and A2 scenarios, respectively. In the case of CMIP5 GCM ensembles, the range of median increases in 2071-2100 are 5% to 15%, 3% to 18% and -3% to 24% for RCP 2.6, 4.5 and 8.5, respectively. The maximum increase ranges are 15% to 53%, 21% to 52% and 22% to 74% for RCP 2.6, 4.5 and 8.5, respectively.

The results of this study are affected by a number of different sources of uncertainties, which arise from emissions uncertainty, model structure, and climate variability. The methodology of using projection ensembles based on a range of possible emission, multiple GCMs, and multiple runs per GCM explicitly and addresses uncertainty in the climate projections. However, long return period events (e.g. > 1000 year) are particularly affected by uncertainties due to sampling variability, and the results for long return period events presented in this report should be treated with a caution.

For future research, the streamflow extremes for CMIP5 should be updated with the CMIP5 GCM driven VIC model simulations. While the GEVcdn model provides a robust statistical methodology for evaluating the parameters of the GEV distribution based on climatic covariates, the CMIP5 GCM driven VIC simulations will provide a means for directly estimating the GEV parameters for future peak flow distributions. The generation of hydrologic projections using the VIC model is part of PCIC's work plan, but the process is resource intensive and will likely require several years. Nevertheless, the use of such direct methodology could potentially reduce uncertainties in the projected streamflow extremes. Future research should also focus on ascertaining a clearer understanding of the physical mechanisms which drive annual maximum peak flow events, particularly extremely rare events. A more physically-based understanding of peak flow change would lend greater confidence to climate change studies on flood impacts.

REFERENCES

Akaike, H., 1974: A new look at the statistical model identification. *IEEE Trans. Autom. Control*, **19**, 716–723, doi:10.1109/TAC.1974.1100705.

Arora, V. K., and Coauthors, 2011: Carbon emission limits required to satisfy future representative concentration pathways of greenhouse gases. *Geophys. Res. Lett.*, **38**, n/a – n/a, doi:10.1029/2010GL046270.

Bennett, K. E., A. T. Werner, and M. Schnorbus, 2012: Uncertainties in Hydrologic and Climate Change Impact Analyses in Headwater Basins of British Columbia. *J. Clim.*, **25**, 5711–5730, doi:10.1175/JCLI-D-11-00417.1.

Beven, K., 2006: A manifesto for the equifinality thesis. *J. Hydrol.*, **320**, 18–36, doi:10.1016/j.jhydrol.2005.07.007.

Cannon, A. J., 2010: A flexible nonlinear modelling framework for nonstationary generalized extreme value analysis in hydroclimatology. *Hydrol. Process.*, **24**, 673–685, doi:10.1002/hyp.7506.

——, 2011: GEVcdn: An R package for nonstationary extreme value analysis by generalized extreme value conditional density estimation network. *Comput. Geosci.*, **37**, 1532–1533, doi:10.1016/j.cageo.2011.03.005.

——, 2014: *GEVcdn: GEV conditional density estimation network*. http://cran.r-project.org/web/packages/GEVcdn/index.html (Accessed January 22, 2015).

Coles, S., 2001: *An Introduction to Statistical Modeling of Extreme Values*. Springer Science & Business Media, 226 pp.

Condon, L. E., S. Gangopadhyay, and T. Pruitt, 2015: Climate change and non-stationary flood risk for the upper Truckee River basin. *Hydrol Earth Syst Sci*, **19**, 159–175, doi:10.5194/hess-19-159-2015.

Cooley, D., 2013: Return Periods and Return Levels Under Climate Change. *Extremes in a Changing Climate*, A. AghaKouchak, D. Easterling, K. Hsu, S. Schubert, and S. Sorooshian, Eds., *Water Science and Technology Library*, Springer Netherlands, 97–114 http://link.springer.com/chapter/10.1007/978-94-007-4479-0_4 (Accessed April 17, 2015).

Deser, C., A. Phillips, V. Bourdette, and H. Teng, 2012: Uncertainty in climate change projections: the role of internal variability. *Clim. Dyn.*, **38**, 527–546, doi:10.1007/s00382-010-0977-x.

Edenhofer, O., and Coauthors, eds., 2014: Climate change 2014: Mitigation of climate change. *Work. Group III Contrib. Fifth Assess. Rep. Intergov. Panel Clim. Change UK N. Y.*,. http://report.mitigation2014.org/spm/ipcc_wg3_ar5_summary-for-policymakers_may-version.pdf (Accessed April 22, 2015).

Flood Safety Section, 2014: *Simulating the Effects of Sea Level Rise and Climate Change on Fraser River Flood Scenarios*. BC Ministry of Forests, Lands and Natural Resource Operations, Surrey, BC, http://www.env.gov.bc.ca/wsd/public_safety/flood/pdfs_word/Simulating_Effects_of_Sea_Level_Rise_and_Climate_Change_on_Fraser_Flood_Scenarios_Final_Report_May-2014.pdf.

Friederichs, P., and A. Hense, 2007: Statistical Downscaling of Extreme Precipitation Events Using Censored Quantile Regression. *Mon. Weather Rev.*, **135**, 2365–2378, doi:10.1175/MWR3403.1.

Friederichs, P., and A. Hense, 2008: A Probabilistic Forecast Approach for Daily Precipitation Totals. *Weather Forecast.*, **23**, 659–673, doi:10.1175/2007WAF2007051.1.

Hirsch, R. M., and J. R. Stedinger, 1987: Plotting positions for historical floods and their precision. *Water Resour. Res.*, **23**, 715–727, doi:10.1029/WR023i004p00715.

Huntington, T. G., 2006: Evidence for intensification of the global water cycle: Review and synthesis. *J. Hydrol.*, **319**, 83–95, doi:10.1016/j.jhydrol.2005.07.003.

Hurvich, C. M., and C.-L. Tsai, 1989: Regression and time series model selection in small samples. *Biometrika*, **76**, 297–307, doi:10.1093/biomet/76.2.297.

Katz, R. W., 2013: Statistical Methods for Nonstationary Extremes. *Extremes in a Changing Climate*, A. AghaKouchak, D. Easterling, K. Hsu, S. Schubert, and S. Sorooshian, Eds., *Water Science and Technology Library*, Springer Netherlands, 15–37 http://link.springer.com/chapter/10.1007/978-94-007-4479-0_2 (Accessed January 21, 2015).

Kay, A. L., H. N. Davies, V. A. Bell, and R. G. Jones, 2008: Comparison of uncertainty sources for climate change impacts: flood frequency in England. *Clim. Change*, **92**, 41–63, doi:10.1007/s10584-008-9471-4.

Kendon, E. J., R. G. Jones, E. Kjellström, and J. M. Murphy, 2010: Using and Designing GCM–RCM Ensemble Regional Climate Projections. *J. Clim.*, **23**, 6485–6503, doi:10.1175/2010JCLI3502.1.

Kharin, V. V., and F. W. Zwiers, 2005: Estimating Extremes in Transient Climate Change Simulations. *J. Clim.*, **18**, 1156–1173, doi:10.1175/JCLI3320.1.

Kharin, V. V., F. W. Zwiers, X. Zhang, and M. Wehner, 2013: Changes in temperature and precipitation extremes in the CMIP5 ensemble. *Clim. Change*, **119**, 345–357, doi:10.1007/s10584-013-0705-8.

Knutti, R., and J. Sedláček, 2013: Robustness and uncertainties in the new CMIP5 climate model projections. *Nat. Clim. Change*, **3**, 369–373, doi:10.1038/nclimate1716.

Moss, R. H., and Coauthors, 2008: *Towards New Scenarios for Analysis of Emissions, Climate Change, Impacts, and Response Strategies*. Pacific Northwest National Laboratory (PNNL), Richland, WA (US), http://www.osti.gov/scitech/biblio/940991 (Accessed April 22, 2015).

——, and Coauthors, 2010: The next generation of scenarios for climate change research and assessment. *Nature*, **463**, 747–756, doi:10.1038/nature08823.

Nakićenović, N., and R. Swart, eds., 2000: *Special report on emissions scenarios: a special report of working group III of the Intergovernmental Panel on Climate Change*. Cambridge University Press,.

Northwest Hydraulic Consultants, 2008: *Comprehensive review of Fraser at Hope flood hydrology and flows - Scoping Study*. Surrey, BC, http://www.env.gov.bc.ca/wsd/public_safety/flood/pdfs_word/review_fraser_flood_flows_hope.pdf.

Payrastre, O., E. Gaume, and H. Andrieu, 2011: Usefulness of historical information for flood frequency analyses: Developments based on a case study. *Water Resour. Res.*, **47**, W08511, doi:10.1029/2010WR009812.

Phien, H. N., 1987: A review of methods of parameter estimation for the extreme value type-1 distribution. *J. Hydrol.*, **90**, 251–268, doi:10.1016/0022-1694(87)90070-9.

Prudhomme, C., and H. Davies, 2008a: Assessing uncertainties in climate change impact analyses on the river flow regimes in the UK. Part 2: future climate. *Clim. Change*, **93**, 197–222, doi:10.1007/s10584-008-9461-6.

——, and ——, 2008b: Assessing uncertainties in climate change impact analyses on the river flow regimes in the UK. Part 2: future climate. *Clim. Change*, **93**, 197–222, doi:10.1007/s10584-008-9461-6.

Salas, J., and J. Obeysekera, 2014: Revisiting the Concepts of Return Period and Risk for Nonstationary Hydrologic Extreme Events. *J. Hydrol. Eng.*, **19**, 554–568, doi:10.1061/(ASCE)HE.1943-5584.0000820.

Schnorbus, M., A. Werner, and K. Bennett, 2014: Impacts of climate change in three hydrologic regimes in British Columbia, Canada. *Hydrol. Process.*, **28**, 1170–1189, doi:10.1002/hyp.9661.

Schnorbus, M. A., and A. J. Cannon, 2014: Statistical emulation of streamflow projections from a distributed hydrological model: Application to CMIP3 and CMIP5 climate projections for British Columbia, Canada. *Water Resour. Res.*, n/a – n/a, doi:10.1002/2014WR015279.

Shrestha, R. R., M. A. Schnorbus, A. T. Werner, and A. J. Berland, 2012: Modelling spatial and temporal variability of hydrologic impacts of climate change in the Fraser River basin, British Columbia, Canada. *Hydrol. Process.*, **26**, 1840–1860, doi:10.1002/hyp.9283.

——, D. L. Peters, and M. A. Schnorbus, 2014: Evaluating the ability of a hydrologic model to replicate hydro-ecologically relevant indicators. *Hydrol. Process.*, **28**, 4294–4310, doi:10.1002/hyp.9997.

Solomon, S., D. Qin, M. Manning, Z Chen, M. Marquis, K. Averyt, M. Tignor, and Miller, eds., 2007: *Climate change 2007-the physical science basis: Working group I contribution to the fourth assessment report of the IPCC*. Cambridge University Press,.

Stedinger, J. R., R. M. Vogel, and E. Foufoula-Georgiou, 1993: Frequency analysis of extreme events. *Handbook of Hydrology*, D.R. Maidment, Ed., McGraw-Hill, United States, p. 1424.

Towler, E., B. Rajagopalan, E. Gilleland, R. S. Summers, D. Yates, and R. W. Katz, 2010: Modeling hydrologic and water quality extremes in a changing climate: A statistical approach based on extreme value theory. *Water Resour. Res.*, **46**, W11504, doi:10.1029/2009WR008876.

Vasiliades, L., P. Galiatsatou, and A. Loukas, 2014: Nonstationary Frequency Analysis of Annual Maximum Rainfall Using Climate Covariates. *Water Resour. Manag.*, **29**, 339–358, doi:10.1007/s11269-014-0761-5.

Van Vuuren, D. P., and Coauthors, 2011: The representative concentration pathways: an overview. *Clim. Change*, **109**, 5–31, doi:10.1007/s10584-011-0148-z.

Wilks, D. S., 2006: *Statistical Methods in the Atmospheric Sciences: An Introduction*. Academic Press, 650 pp.

Zhang, X., J. Wang, F. W. Zwiers, and P. Y. Groisman, 2010: The Influence of Large-Scale Climate Variability on Winter Maximum Daily Precipitation over North America. *J. Clim.*, **23**, 2902–2915, doi:10.1175/2010JCLI3249.1.

LIST OF TABLES

LIST OF FIGURES

APPENDIX A: EMISSIONS SCENARIOS

A1. Special Report on Emissions Scenarios (SRES)

SRES scenarios are emission scenarios, developed by Nakićenović and Swart (2000), are used as the basis for climate projections for phase 3 of the Coupled Model Intercomparison Project (CMIP3). A brief description of the SRES scenarios from Nakićenović and Swart (2000), which are used in this report is given below:

- The **A1** storyline and scenario family describes a future world of very rapid economic growth, global population that peaks in mid-century and declines thereafter, and the rapid introduction of new and more efficient technologies. Major underlying themes are convergence among regions, capacity building, and increased cultural and social interactions, with a substantial reduction in regional differences in per capita income. The A1 scenario family develops into three groups that describe alternative directions of technological change in the energy system. The three A1 groups are distinguished by their technological emphasis: fossil intensive (A1FI), non-fossil energy sources (A1T), or a balance across all sources (**A1B**).
- The **B1** storyline and scenario family describes a convergent world with the same global population that peaks in mid-century and declines thereafter, as in the A1 storyline, but with rapid changes in economic structures toward a service and information economy, with reductions in material intensity, and the introduction of clean and resource-efficient technologies. The emphasis is on global solutions to economic, social, and environmental sustainability, including improved equity, but without additional climate initiatives.
- The **A2** storyline and scenario family describes a very heterogeneous world. The underlying theme is self-reliance and preservation of local identities. Fertility patterns across regions converge very slowly, which results in continuously increasing global population. Economic development is primarily regionally oriented and per capita economic growth and technological change are more fragmented and slower than in other storylines.

A2. Representative Concentration Pathways (RCPs)

The RCP emissions scenarios provide the radiative forcing conditions for phase 5 of the Coupled Model Intercomparison Project (CMIP5). RCP scenarios include time series of emissions and concentrations of the full suite of greenhouse gases (GHGs) and aerosols and chemically active gases, as well as land use / land cover (Moss et al. 2008). The word representative signifies that each RCP provides only one of many possible scenarios that would lead to the specific radiative forcing characteristics. The term pathway emphasizes that not only the long-term concentration levels are of interest, but also the trajectory taken over time to reach that outcome (Moss et al. 2010). A brief description of the RCPs from IPCC WGIII Glossary (Edenhofer et al. 2014), which are used in this report is given below:

- **RCP2.6** is a pathway where radiative forcing peaks at approximately 3 W m^{-2} before 2100 and then declines.
- **RCP4.5** is an intermediate stabilization pathway in which radiative forcing is stabilized at approximately 4.5 W m^{-2} after 2100.

- **RCP8.5** is a high pathway for which radiative forcing reaches greater than 8.5 W m^{-2} by 2100 and continues to rise for some amount of time.

A3. CMIP3 vs CMIP5 Projections

This study used climate projections derived from CMIP3 SRES scenarios and CMIP5 RCPs. It is important to note that the SRES scenarios and RCPs do not provide equivalent projections. For instance, the SRES A2 scenario represents a high emissions scenario, with diagnosed radiative forcing of 8–9.5 W m^{-2} over preindustrial levels by the end of the 21st century (based on the mean plus-or-minus one standard deviation from a simple climate model tuned to 19 CMIP3 GCMs) (Solomon et al. 2007). The RCP8.5 scenario is also representative of high emissions scenarios (with radiative forcing greater than 8.5 W m^{-2}) in which no climate policies have been implemented and which represents the worst-case of the four RCP scenarios. RCP8.5. Despite similar radiative forcing by 2100, the emissions trajectories and composition of greenhouse gasses and pollutants prescribed by the two scenarios are not identical and are, therefore, not expected to generate an identical climate response (Knutti and Sedláček 2013).

Developers of RCP scenarios do not assign any preference to one RCP compared with others (van Vuuren et al. 2011) . However studies (e.g., Arora et al. 2011) suggest there is little room to limit the warming associated with the RCP 2.6 scenario. A comparison of the change in global mean temperature over the twentieth and twenty-first century as simulated by the CMIP3 and CMIP5 models is shown in Figure A1 (Knutti and Sedláček 2013).

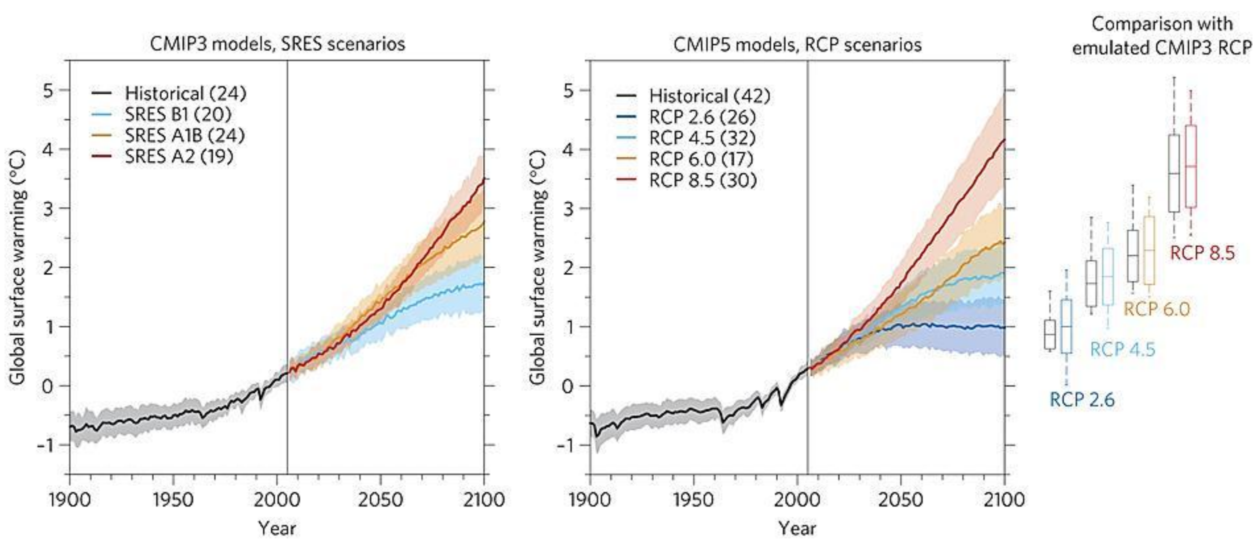

Figure A1. Global temperature change and uncertainty. Global temperature change (mean and one standard deviation as shading) relative to 1986–2005 for the SRES scenarios run by CMIP3 and the RCP scenarios run by CMIP5. The number of models is given in brackets. The box plots (mean, one standard deviation, and minimum to maximum range) are given for 2080–2099 for CMIP5 (colours) and for the model calibrated to 19 CMIP3 models (black), both running the RCP scenarios (Source: Knutti and Sedláček 2013).

APPENDIX B: TABLES

Table B1. Annual maximum flow data and plotting positions for Fraser River at Hope (WSC 08MF005)

Year	Discharge (m^3/s)	Plotting position, $\hat{p}_i$	Empirical return period ($1/\hat{p}_i$)	Record type
1912	7420	0.770	1.30	Systematic
1913	10300	0.192	5.21	Systematic
1914	8550	0.450	2.22	Systematic
1915	5800	0.984	1.02	Systematic
1916	8720	0.411	2.44	Systematic
1917	8980	0.391	2.56	Systematic
1918	9770	0.274	3.64	Systematic
1919	8520	0.459	2.18	Systematic
1920	10800	0.114	8.78	Systematic
1921	11100	0.080	12.51	Systematic
1922	9910	0.236	4.25	Systematic
1923	9260	0.362	2.76	Systematic
1924	9680	0.299	3.35	Systematic
1925	9970	0.226	4.43	Systematic
1926	6000	0.965	1.04	Systematic
1927	8670	0.425	2.35	Systematic
1928	10300	0.192	5.21	Systematic
1929	8040	0.595	1.68	Systematic
1930	7840	0.654	1.53	Systematic
1931	7620	0.722	1.39	Systematic
1932	8500	0.484	2.07	Systematic
1933	9290	0.352	2.84	Systematic
1934	8500	0.484	2.07	Systematic
1935	8040	0.595	1.68	Systematic
1936	10600	0.158	6.34	Systematic
1937	7480	0.751	1.33	Systematic
1938	6820	0.897	1.11	Systematic
1939	7820	0.673	1.49	Systematic
1940	7080	0.858	1.17	Systematic
1941	5130	0.994	1.01	Systematic
1942	7220	0.805	1.24	Systematic
1943	7560	0.732	1.37	Systematic
1944	6060	0.955	1.05	Systematic
1945	7820	0.673	1.49	Systematic
1946	9540	0.313	3.19	Systematic
1947	8160	0.566	1.77	Systematic
1948	15200	0.012	84.58	Systematic

Year	Discharge (m^3/s)	Plotting position, $\hat{p}_i$	Empirical return period $(1/\hat{p}_i)$	Record type
1949	9000	0.381	2.62	Systematic
1950	12500	0.031	31.97	Systematic
1951	8040	0.595	1.68	Systematic
1952	8330	0.537	1.86	Systematic
1953	7220	0.805	1.24	Systematic
1954	9060	0.372	2.69	Systematic
1955	11300	0.065	15.31	Systematic
1956	9680	0.299	3.35	Systematic
1957	10400	0.177	5.64	Systematic
1958	9770	0.274	3.64	Systematic
1959	8470	0.508	1.97	Systematic
1960	9340	0.343	2.92	Systematic
1961	9510	0.323	3.10	Systematic
1962	8210	0.556	1.80	Systematic
1963	7700	0.693	1.44	Systematic
1964	11600	0.051	19.71	Systematic
1965	8580	0.440	2.27	Systematic
1966	7900	0.644	1.55	Systematic
1967	10800	0.114	8.78	Systematic
1968	8830	0.401	2.49	Systematic
1969	7820	0.673	1.49	Systematic
1970	8670	0.425	2.35	Systematic
1971	8500	0.484	2.07	Systematic
1972	12900	0.022	46.40	Systematic
1973	7960	0.634	1.58	Systematic
1974	10800	0.114	8.78	Systematic
1975	7650	0.707	1.41	Systematic
1976	9400	0.333	3.00	Systematic
1977	6770	0.907	1.10	Systematic
1978	6970	0.877	1.14	Systematic
1979	8390	0.518	1.93	Systematic
1980	6070	0.946	1.06	Systematic
1981	8370	0.527	1.90	Systematic
1982	9780	0.255	3.92	Systematic
1983	7280	0.790	1.27	Systematic
1984	8270	0.547	1.83	Systematic
1985	9770	0.274	3.64	Systematic
1986	10600	0.158	6.34	Systematic
1987	7180	0.829	1.21	Systematic
1988	7650	0.707	1.41	Systematic
1989	7110	0.848	1.18	Systematic

Year	Discharge (m^3/s)	Plotting position, $\hat{p}_i$	Empirical return period $(1/\hat{p}_i)$	Record type
1990	10100	0.216	4.63	Systematic
1991	8010	0.615	1.63	Systematic
1992	6670	0.926	1.08	Systematic
1993	8500	0.484	2.07	Systematic
1994	7000	0.868	1.15	Systematic
1995	6840	0.887	1.13	Systematic
1996	8100	0.576	1.74	Systematic
1997	11300	0.065	15.31	Systematic
1998	6710	0.916	1.09	Systematic
1999	11000	0.090	11.16	Systematic
2000	8000	0.625	1.60	Systematic
2001	7140	0.839	1.19	Systematic
2002	10600	0.158	6.34	Systematic
2003	7300	0.780	1.28	Systematic
2004	6650	0.936	1.07	Systematic
2005	7460	0.761	1.31	Systematic
2006	7190	0.819	1.22	Systematic
2007	10800	0.114	8.78	Systematic
2008	10200	0.206	4.85	Systematic
2009	7490	0.741	1.35	Systematic
2010	5950	0.975	1.03	Systematic
2011	9850	0.245	4.08	Systematic
2012	11700	0.041	24.39	Systematic
2013	10700	0.138	7.23	Systematic
1894	17000	0.003	334.00	Historic

Table B2. Summary of CMIP3 Global Climate Model ensemble

GCM Name[a]	Number of Runs by SRES Scenario		
	B1	A1B	A2
CCSM3	1	1	1
CGCM3.1 T47	1	1	1
CSIRO Mk3.5	1	1	1
ECHAM5	1	1	1
GFDL CM 2.1	1	1	1
HadCM3	1	1	1
HadGEM1		1	1
MIROC3.2(medres)	1	1	1
TOTAL	7	8	8

[a] See http://www-pcmdi.llnl.gov/ipcc/model_documentation/ipcc_model_documentation.php for a list of official model names and modelling institution.

Table B3. Summary of CMIP5 Global Climate Model ensemble

GCM Name[a]	Number of Runs by RCP Scenario		
	RCP2.6	RCP4.5	RCP8.5
ACCESS1.0		1	1
ACCESS1.3		1	1
BCC-CSM1.1	1	1	1
BCC-CSM1.1(m)	1	1	1
BNU-ESM	1	1	1
CanESM2	5	5	5
CCSM4	3	3	3
CMCC-CM		1	1
CMCC-CMS		1	1
CNRM-CM5-2	1	1	1
CSIRO-Mk3.6.0	10	10	10
EC-EARTH		1	1
FGOALS-g2	1	1	1
FGOALS-s2	1	3	3
GFDL-ESM2G	1	1	1
GFDL-ESM2M	1	1	1
HadGEM2-CC		1	1
HadGEM2-ES	4	4	4
INM-CM4		1	1
IPSL-CM5A-LR	4	4	4
IPSL-CM5A-MR	1	1	1
IPSL-CM5B-LR		1	1
MIROC5	3	3	3
MIROC5-ESM	1	1	1
MIROC5-ESM-CHEM	1	1	1
MPI-ESM-LR	3	3	3
MPI-ESM-MR	1	1	1
MRI-CGCM3	1	1	1
NorESM1-M	1	1	1
TOTAL	46	56	56

[a] See http://cmip-pcmdi.llnl.gov/cmip5/availability.html for a list of official model names and modelling institution.

Table B4. Percentage change in discharge quantiles for the three future periods against the historical period of 1961-1990. The results are for CMIP3 GCMs.

Scenario	Future period	GCM	% change in quantile discharge for return periods								
			10	**50**	**100**	**200**	**500**	**1000**	**2000**	**5000**	**10000**
B1	2011-2040	CCSM3	-2	1	2	3	4	5	6	7	8
		CGCM3.1 T47	0	3	4	5	6	7	8	9	10
		CSIRO Mk3.5	1	3	3	4	5	6	7	8	9
		ECHAM5	7	9	9	10	10	11	11	12	12
		GFDL CM2.1	4	6	7	8	8	9	9	10	10
		HadCM3	10	12	13	14	15	16	16	17	17
		MIROC3.2(medres)	6	9	11	12	14	15	17	18	20
	2041-2070	CCSM3	0	4	5	6	7	9	10	11	12
		CGCM3.1 T47	13	18	19	21	23	24	26	28	29
		CSIRO Mk3.5	6	9	10	11	12	13	14	15	16
		ECHAM5	13	17	19	20	21	22	23	25	25
		GFDL CM2.1	3	8	10	12	14	16	18	20	22
		HadCM3	14	19	20	22	24	25	27	29	30
		MIROC3.2(medres)	9	14	16	18	21	22	24	26	27
	2071-2098	CCSM3	0	4	5	7	8	9	11	12	13
		CGCM3.1 T47	11	19	22	25	29	31	34	38	41
		CSIRO Mk3.5	4	7	8	9	10	11	12	13	14
		ECHAM5	14	19	21	23	25	26	28	29	31
		GFDL CM2.1	9	15	17	19	22	23	25	27	29
		HadCM3	12	16	18	19	20	21	22	23	24
		MIROC3.2(medres)	8	12	14	16	18	19	20	22	23
A1B	2011-2040	CCSM3	7	10	11	11	12	13	14	14	15
		CGCM3.1 T47	8	10	10	11	11	12	12	13	13
		CSIRO Mk3.5	2	3	3	3	3	3	3	4	4
		ECHAM5	9	13	15	17	19	20	22	24	25
		GFDL CM2.1	1	3	4	5	6	6	7	8	8
		HadCM3	13	19	21	24	27	29	31	34	36
		HadGEM1	4	6	6	7	7	8	8	8	9
		MIROC3.2(medres)	1	4	5	6	8	9	10	11	12
	2041-2070	CCSM3	7	15	18	21	25	28	31	34	37
		CGCM3.1 T47	17	22	23	24	25	26	27	28	29
		CSIRO Mk3.5	1	3	3	4	5	6	7	8	8
		ECHAM5	5	7	8	8	9	10	10	11	11
		GFDL CM2.1	0	4	6	8	10	12	14	16	18
		HadCM3	14	20	22	24	27	28	30	32	34
		HadGEM1	-1	4	6	8	11	13	14	17	19
		MIROC3.2(medres)	6	11	13	15	18	20	21	24	25
	2071-2098	CCSM3	3	9	11	13	15	17	19	21	22
		CGCM3.1 T47	9	17	20	23	26	29	32	35	38
		CSIRO Mk3.5	6	9	10	11	13	13	14	15	16
		ECHAM5	8	11	12	14	15	16	16	17	18
		GFDL CM2.1	-3	0	1	3	4	5	6	7	8
		HadCM3	15	20	22	23	25	27	28	29	31
		HadGEM1	2	8	10	12	14	15	16	17	18
		MIROC3.2(medres)	14	24	28	31	36	40	44	48	52
A2	2011-2040	CCSM3	5	11	13	15	18	20	21	24	25
		CGCM3.1 T47	12	16	18	19	20	21	22	23	23

Scenario	Future period	GCM	% change in quantile discharge for return periods								
			10	50	100	200	500	1000	2000	5000	10000
		CSIRO Mk3.5	3	4	4	4	4	4	4	4	4
		ECHAM5	12	18	20	23	26	28	31	34	36
		GFDL CM2.1	-1	2	4	5	7	8	10	11	13
		HadCM3	11	15	17	18	20	22	23	25	26
		HadGEM1	3	6	7	8	9	10	11	12	12
		MIROC3.2(medres)	7	12	14	17	20	22	24	26	28
	2041-2070	CCSM3	-3	0	2	3	5	6	7	8	9
		CGCM3.1 T47	15	21	23	25	28	29	31	33	34
		CSIRO Mk3.5	1	5	7	8	10	12	13	15	16
		ECHAM5	9	14	16	18	20	21	23	25	26
		GFDL CM2.1	3	7	9	11	13	14	16	18	20
		HadCM3	11	14	15	16	17	17	18	19	19
		HadGEM1	0	4	5	7	8	9	10	11	12
		MIROC3.2(medres)	13	18	19	21	22	23	24	26	26
	2071-2098	CCSM3	-3	6	10	14	19	22	26	31	34
		CGCM3.1 T47	18	26	29	32	36	39	41	45	47
		CSIRO Mk3.5	3	9	11	13	15	17	19	21	23
		ECHAM5	12	22	25	29	33	36	39	43	45
		GFDL CM2.1	4	11	14	16	20	23	25	28	31
		HadCM3	17	22	24	25	27	28	29	30	31
		HadGEM1	3	14	18	23	28	32	36	40	44
		MIROC3.2(medres)	25	37	41	46	53	58	63	70	75

Table B5. Discharge quantiles for the three future periods for the CMIP3 GCMs.

Scenario	Future period	GCM	Quantile discharge for return periods (m^3/s)								
			10	50	100	200	500	1000	2000	5000	10000
Historic, GEV type I			11222	13632	14650	15665	17004	18016	17798	18985	21376
B1	2011-2040	CCSM3	11040	13710	14877	16060	17649	18869	20104	21758	23023
		CGCM3.1 T47	11230	14020	15224	16437	18057	19294	20540	22202	23468
		CSIRO Mk3.5	11285	13986	15158	16340	17922	19133	20355	21986	23231
		ECHAM5	11992	14816	16010	17200	18771	19958	21146	22716	23904
		GFDL CM2.1	11690	14476	15664	16853	18428	19623	20822	22411	23616
		HadCM3	12307	15323	16598	17868	19545	20812	22079	23754	25021
		MIROC3.2 (medres)	11914	14898	16216	17560	19377	20781	22209	24131	25610
	2041-2070	CCSM3	11271	14117	15354	16604	18277	19559	20854	22584	23905
		CGCM3.1 T47	12683	16030	17483	18952	20919	22427	23950	25986	27542
		CSIRO Mk3.5	11942	14858	16121	17395	19098	20401	21715	23469	24807
		ECHAM5	12700	15965	17363	18764	20627	22044	23468	25359	26796
		GFDL CM2.1	11611	14752	16136	17546	19451	20923	22421	24436	25986
		HadCM3	12844	16167	17618	19089	21066	22584	24122	26182	27759
		MIROC3.2 (medres)	12178	15564	17030	18510	20491	22007	23538	25582	27143
	2071-2098	CCSM3	11203	14170	15443	16723	18426	19723	21028	22762	24081
		CGCM3.1 T47	12460	16171	17832	19539	21869	23686	25549	28081	30046
		CSIRO Mk3.5	11725	14559	15794	17042	18717	20001	21299	23036	24364
		ECHAM5	12789	16237	17725	19223	21224	22753	24294	26349	27915
		GFDL CM2.1	12274	15655	17137	18642	20669	22230	23814	25942	27574
		HadCM3	12625	15879	17262	18645	20476	21864	23255	25097	26494
		MIROC3.2 (medres)	12107	15313	16703	18106	19982	21419	22869	24806	26284
A1B	2011-2040	CCSM3	12038	14968	16213	17458	19105	20353	21604	23261	24517
		CGCM3.1 T47	12101	14968	16175	17376	18958	20152	21344	22917	24105
		CSIRO Mk3.5	11489	14037	15109	16175	17578	18636	19693	21087	22141
		ECHAM5	12230	15459	16869	18298	20219	21696	23194	25204	26745
		GFDL CM2.1	11341	14055	15221	16392	17951	19139	20333	21920	23127
		HadCM3	12730	16235	17798	19401	21582	23278	25011	27357	29171
		HadGEM1	11658	14431	15595	16752	18274	19421	20565	22074	23213
		MIROC3.2 (medres)	11365	14184	15417	16667	18345	19634	20938	22682	24015
	2041-2070	CCSM3	12031	15685	17312	18982	21256	23027	24840	27300	29206
		CGCM3.1 T47	13185	16574	18010	19444	21340	22775	24211	26111	27550
		CSIRO Mk3.5	11324	13987	15145	16315	17884	19088	20305	21933	23178
		ECHAM5	11793	14585	15774	16964	18540	19735	20934	22524	23730
		GFDL CM2.1	11256	14233	15561	16922	18774	20214	21685	23676	25215
		HadCM3	12838	16378	17914	19467	21547	23141	24751	26903	28547
		HadGEM1	11075	14161	15527	16922	18815	20282	21779	23802	25363
		MIROC3.2 (medres)	11908	15150	16583	18043	20017	21542	23092	25178	26781
	2071-2098	CCSM3	11529	14804	16226	17663	19590	21068	22563	24564	26094
		CGCM3.1 T47	12259	15890	17517	19191	21477	23262	25095	27587	29525
		CSIRO Mk3.5	11868	14865	16145	17428	19132	20427	21729	23458	24772
		ECHAM5	12093	15174	16481	17788	19516	20827	22140	23879	25197
		GFDL CM2.1	10859	13666	14869	16079	17687	18912	20144	21782	23028
		HadCM3	12865	16354	17846	19342	21329	22839	24357	26372	27902
		HadGEM1	11490	14770	16152	17527	19339	20708	22075	23881	25246
		MIROC3.2 (medres)	12819	16869	18701	20595	23196	25235	27334	30198	32428
A2	2011-	CCSM3	11827	15093	16536	18007	19997	21534	23097	25201	26817

Scenario	Future period	GCM	Quantile discharge for return periods (m^3/s)								
			10	**50**	**100**	**200**	**500**	**1000**	**2000**	**5000**	**10000**
	2040	CGCM3.1 T47	12607	15844	17217	18588	20399	21770	23143	24959	26335
		CSIRO Mk3.5	11589	14131	15206	16278	17692	18761	19830	21243	22312
		ECHAM5	12546	16067	17638	19249	21442	23147	24889	27247	29069
		GFDL CM2.1	11137	13970	15218	16490	18206	19530	20874	22681	24068
		HadCM3	12496	15675	17076	18504	20431	21919	23430	25462	27023
		HadGEM1	11601	14445	15670	16901	18543	19794	21053	22728	24002
		MIROC3.2 (medres)	11979	15292	16766	18275	20326	21917	23542	25737	27432
	2041-2070	CCSM3	10884	13683	14899	16127	17771	19030	20299	21994	23287
		CGCM3.1 T47	12952	16530	18075	19633	21714	23304	24908	27048	28680
		CSIRO Mk3.5	11359	14329	15634	16961	18750	20130	21532	23417	24865
		ECHAM5	12261	15527	16957	18410	20365	21869	23393	25437	27002
		GFDL CM2.1	11535	14595	15946	17324	19187	20626	22090	24060	25574
		HadCM3	12467	15518	16817	18118	19841	21148	22458	24195	25511
		HadGEM1	11224	14174	15436	16701	18380	19657	20939	22641	23933
		MIROC3.2 (medres)	12656	16037	17473	18907	20804	22242	23682	25588	27032
	2071-2098	CCSM3	10837	14454	16102	17812	20171	22029	23950	26581	28639
		CGCM3.1 T47	13269	17226	18969	20746	23148	25005	26895	29442	31403
		CSIRO Mk3.5	11570	14808	16226	17665	19604	21098	22615	24653	26217
		ECHAM5	12557	16604	18385	20200	22653	24549	26478	29076	31074
		GFDL CM2.1	11622	15098	16647	18235	20394	22073	23788	26111	27906
		HadCM3	13096	16615	18110	19604	21580	23078	24579	26565	28070
		HadGEM1	11566	15560	17357	19212	21754	23744	25792	28584	30758
		MIROC3.2 (medres)	14059	18613	20727	22943	26037	28503	31076	34643	37465

Table B6. Percentage change in discharge quantiles for the three future periods against the historical period of 1961-1990. The results are for selected CMIP5 GCMs

Scenario	Future period	GCM	% change in quantile discharge for return periods								
			10	50	100	200	500	1000	2000	5000	10000
RCP2.6	2011-2040	BCC-CSM1.1(m)	4	6	7	8	9	9	10	10	11
		BNU-ESM	-2	4	6	8	11	14	16	19	22
		CanESM2	4	9	11	13	16	17	19	21	23
		CCSM4	-1	-1	0	0	1	1	2	2	3
		CNRM-CM5	1	5	6	8	10	12	13	16	17
		CSIRO-Mk3.6.0	9	12	14	15	17	19	20	22	23
		FGOALS-g2	1	3	3	4	5	5	6	6	7
		GFDL-ESM2G	-1	0	1	1	2	2	3	3	4
		HadGEM12-ES	4	11	14	17	22	25	28	33	36
		IPSL-CM5A-LR	-4	-1	0	1	2	3	4	5	6
		MIROC5	0	9	12	16	21	25	28	33	36
		MPI-ESM-LR	2	4	5	6	6	7	7	8	8
		MRI-CGCM3	5	5	5	6	6	6	6	6	6
		NorESM1-M	4	12	16	20	26	30	35	42	47
	2041-2070	BCC-CSM1.1(m)	3	4	5	5	6	6	6	6	6
		BNU-ESM	8	11	12	13	13	14	14	15	15
		CanESM2	7	13	15	17	20	22	24	26	28
		CCSM4	1	2	2	3	3	4	4	5	6
		CNRM-CM5	13	17	19	21	23	24	25	27	28
		CSIRO-Mk3.6.0	7	13	15	18	21	24	26	29	32
		FGOALS-g2	18	28	32	37	42	46	51	56	60
		GFDL-ESM2G	6	7	8	9	10	11	12	13	14
		HadGEM12-ES	5	9	11	13	15	17	18	20	22
		IPSL-CM5A-LR	0	3	4	5	6	7	8	9	9
		MIROC5	8	15	18	21	25	28	30	34	36
		MPI-ESM-LR	1	3	4	5	6	6	7	7	7
		MRI-CGCM3	1	2	2	2	2	2	2	2	2
		NorESM1-M	6	10	12	14	16	18	20	22	23
	2071-2100	BCC-CSM1.1(m)	-1	0	1	1	2	2	2	3	3
		BNU-ESM	5	7	7	7	8	8	8	8	8
		CanESM2	4	9	10	12	14	15	16	18	19
		CCSM4	1	0	-1	-2	-3	-3	-4	-5	-5
		CNRM-CM5	6	8	8	9	9	10	10	11	11
		CSIRO-Mk3.6.0	6	9	10	11	12	13	13	14	15
		FGOALS-g2	12	17	19	21	23	25	27	29	30
		GFDL-ESM2G	9	10	10	10	10	10	10	10	10
		HadGEM12-ES	4	8	10	12	14	16	18	20	22
		IPSL-CM5A-LR	1	4	5	6	6	7	7	7	8
		MIROC5	3	7	9	11	13	15	16	18	20
		MPI-ESM-LR	4	8	10	11	12	14	14	16	16
		MRI-CGCM3	0	1	1	1	1	1	1	1	1
		NorESM1-M	6	8	9	10	11	11	12	13	13
RCP4.5	2011-2040	ACCESS1.0	6	14	17	20	24	27	29	33	36
		BCC-CSM1.1(m)	-1	-1	-1	-1	-1	-1	-2	-2	-2
		BNU-ESM	1	0	-1	-2	-3	-3	-4	-5	-5
		CanESM2	-1	2	3	4	5	6	7	7	8
		CCSM4	11	15	16	17	18	19	20	21	21

Scenario	Future period	GCM	% change in quantile discharge for return periods								
			10	50	100	200	500	1000	2000	5000	10000
		CMCC-CM	14	18	19	21	23	24	25	26	28
		CNRM-CM5	6	10	11	13	15	17	18	20	21
		CSIRO-Mk3.6.0	10	19	23	28	33	38	42	49	53
		EC-EARTH	1	4	5	6	6	7	7	7	8
		FGOALS-g2	9	12	13	14	15	16	17	18	19
		GFDL-ESM2G	3	7	9	11	13	15	16	18	20
		HadGEM12-CC	5	5	5	5	5	5	5	5	5
		INM-CM4	5	9	10	11	12	13	14	15	15
		IPSL-CM5A-LR	5	11	13	15	17	19	21	23	25
		MIROC5	5	9	11	13	15	17	19	21	23
		MPI-ESM-LR	-4	-2	-2	-1	-1	0	0	1	1
		MRI-CGCM3	-6	-6	-5	-5	-4	-4	-4	-3	-3
		NorESM1-M	5	6	6	7	7	7	8	8	8
	2041-2070	ACCESS1.0	11	12	13	13	14	14	14	14	14
		BCC-CSM1.1(m)	10	13	14	14	15	15	15	16	16
		BNU-ESM	8	11	13	14	15	16	17	18	19
		CanESM2	5	6	6	7	7	8	8	8	9
		CCSM4	3	8	10	12	14	16	18	21	22
		CMCC-CM	9	12	13	14	16	17	18	19	19
		CNRM-CM5	6	8	9	10	11	12	13	14	15
		CSIRO-Mk3.6.0	2	4	5	5	6	7	7	8	8
		EC-EARTH	3	5	5	6	6	6	6	6	7
		FGOALS-g2	0	4	6	7	9	10	12	13	14
		GFDL-ESM2G	-2	3	5	7	9	11	13	15	17
		HadGEM12-CC	7	8	8	9	9	9	9	9	9
		INM-CM4	1	4	5	6	7	7	8	8	8
		IPSL-CM5A-LR	2	4	5	5	7	7	8	9	10
		MIROC5	1	4	5	6	7	7	8	9	10
		MPI-ESM-LR	2	4	5	6	8	8	9	10	11
		MRI-CGCM3	0	1	2	2	2	2	2	2	3
		NorESM1-M	8	11	11	12	13	13	13	14	14
	2071-2098	ACCESS1.0	14	17	18	19	20	21	22	22	23
		BCC-CSM1.1(m)	2	6	7	8	9	10	11	12	13
		BNU-ESM	0	5	6	8	10	11	13	14	16
		CanESM2	6	10	12	13	15	16	18	19	20
		CCSM4	11	20	24	27	31	34	37	41	44
		CMCC-CM	11	14	15	16	17	18	18	19	20
		CNRM-CM5	15	22	24	27	30	33	35	38	40
		CSIRO-Mk3.6.0	22	25	25	26	27	27	28	28	29
		EC-EARTH	14	17	18	19	20	21	21	22	22
		FGOALS-g2	1	6	8	10	13	15	16	19	20
		GFDL-ESM2G	9	17	19	22	26	28	30	33	35
		HadGEM12-CC	9	11	12	12	13	13	13	14	14
		INM-CM4	-5	1	3	5	8	10	12	14	16
		IPSL-CM5A-LR	2	7	9	11	13	15	17	19	20
		MIROC5	6	11	13	14	16	17	18	20	21
		MPI-ESM-LR	4	12	15	18	22	25	28	32	35
RCP8.5	2011-2040	ACCESS1.0	13	20	23	25	27	29	31	33	35
		BCC-CSM1.1(m)	6	10	11	12	14	15	16	17	18
		BNU-ESM	4	6	7	8	8	9	9	9	10
		CanESM2	8	17	21	25	30	34	38	43	46

Scenario	Future period	GCM	% change in quantile discharge for return periods								
			10	50	100	200	500	1000	2000	5000	10000
		CCSM4	7	13	15	17	20	22	24	26	28
		CMCC-CM	21	28	31	34	38	41	44	48	52
		CNRM-CM5	8	10	11	11	12	12	13	13	13
		CSIRO-Mk3.6.0	12	18	20	22	25	26	28	30	32
		EC-EARTH	5	9	11	12	14	15	17	18	19
		FGOALS-g2	-4	2	5	7	10	12	14	17	19
		GFDL-ESM2G	2	5	6	7	8	8	9	9	9
		HadGEM12-CC	8	9	9	9	9	9	9	8	8
		INM-CM4	-2	10	15	20	26	30	35	41	46
		IPSL-CM5A-LR	-2	4	6	7	10	12	13	15	17
		MIROC5	3	5	6	7	8	8	9	9	10
		MPI-ESM-LR	-5	-5	-5	-5	-5	-4	-4	-4	-4
		MRI-CGCM3	-4	-1	1	2	4	5	6	8	9
		NorESM1-M	13	15	16	17	18	18	19	19	20
	2041-2070	ACCESS1.0	9	13	14	15	16	17	18	18	19
		BCC-CSM1.1(m)	6	10	11	13	14	16	17	18	20
		BNU-ESM	7	13	15	17	20	22	24	27	29
		CanESM2	3	5	6	7	8	9	10	10	11
		CCSM4	2	4	5	6	7	8	9	10	10
		CMCC-CM	0	1	2	3	4	4	5	6	6
		CNRM-CM5	4	7	8	8	10	11	11	12	13
		CSIRO-Mk3.6.0	13	17	18	19	20	20	21	21	21
		EC-EARTH	-3	0	2	3	5	6	8	9	10
		FGOALS-g2	-4	-3	-2	-2	-1	-1	0	1	1
		GFDL-ESM2G	-6	-1	1	3	6	8	10	13	15
		HadGEM12-CC	4	10	13	15	18	20	22	25	27
		INM-CM4	-2	0	1	1	2	2	2	3	3
		IPSL-CM5A-LR	-3	0	2	3	4	5	5	6	7
		MIROC5	1	5	7	8	10	11	11	13	13
		MPI-ESM-LR	-8	-4	-2	-1	1	3	4	6	7
		MRI-CGCM3	-3	2	4	7	9	12	14	16	18
		NorESM1-M	17	20	21	22	23	23	24	24	25
	2071-2098	ACCESS1.0	9	16	19	22	25	28	30	33	35
		BCC-CSM1.1(m)	8	13	14	16	18	20	21	23	25
		BNU-ESM	2	5	6	6	7	8	8	9	9
		CanESM2	9	18	21	25	30	34	38	43	46
		CCSM4	-2	3	5	7	9	11	13	15	17
		CMCC-CM	15	23	27	31	36	39	43	47	51
		CNRM-CM5	6	16	20	25	31	36	41	47	52
		CSIRO-Mk3.6.0	20	25	26	28	29	30	30	31	32
		EC-EARTH	3	9	11	13	16	18	20	22	23
		FGOALS-g2	-5	-1	1	2	4	6	7	9	10
		GFDL-ESM2G	2	7	9	11	13	15	17	18	20
		HadGEM12-CC	-5	-4	-3	-3	-2	-2	-1	-1	-1
		INM-CM4	-5	2	4	6	8	10	11	13	14
		IPSL-CM5A-LR	-5	1	4	6	9	12	14	17	19
		MIROC5	10	18	21	24	27	30	32	34	36
		MPI-ESM-LR	-14	-7	-5	-2	1	4	6	10	12
		MRI-CGCM3	-6	1	4	7	11	14	17	20	23
		NorESM1-M	22	34	39	44	51	56	61	68	73

Table B7. Discharge quantiles for the three future periods for the selected CMIP5 GCMs.

Scenario	Future period	GCM	Quantile Discharge for return periods (m^3/s)								
			10	50	100	200	500	1000	2000	5000	10000
Historic, GEV type I			11222	13632	14650	15665	17004	18016	17798	18985	21376
RCP2.6	2011-2040	BCC-CSM1.1(m)	11630	14473	15677	16879	18468	19672	20876	22470	23677
		BNU-ESM	11041	14114	15504	16942	18918	20470	22071	24261	25972
		CanESM2	11698	14909	16314	17741	19661	21140	22639	24652	26196
		CCSM4	11071	13558	14631	15710	17150	18250	19358	20835	21961
		CNRM-CM5	11378	14267	15563	16895	18710	20123	21569	23528	25043
		CSIRO-Mk3.6.0	12213	15321	16685	18071	19938	21376	22836	24795	26299
		FGOALS-g2	11345	14018	15161	16306	17827	18983	20142	21680	22846
		GFDL-ESM2G	11108	13650	14741	15837	17295	18406	19524	21011	22144
		HadGEM12-ES	11663	15129	16724	18388	20692	22513	24399	26990	29020
		IPSL-CM5A-LR	10761	13480	14650	15828	17397	18593	19798	21401	22621
		MIROC5	11231	14827	16473	18188	20562	22440	24387	27068	29173
		MPI-ESM-LR	11404	14195	15371	16542	18085	19251	20416	21955	23118
		MRI-CGCM3	11789	14361	15452	16540	17977	19065	20154	21594	22685
		NorESM1-M	11624	15217	16932	18761	21364	23478	25723	28895	31455
	2041-2070	BCC-CSM1.1(m)	11546	14245	15374	16493	17962	19068	20169	21619	22713
		BNU-ESM	12104	15127	16387	17635	19270	20498	21720	23328	24539
		CanESM2	11958	15372	16862	18372	20402	21964	23547	25669	27296
		CCSM4	11334	13896	15000	16112	17595	18728	19870	21393	22554
		CNRM-CM5	12709	16013	17447	18895	20833	22316	23813	25812	27337
		CSIRO-Mk3.6.0	12023	15381	16896	18460	20604	22283	24011	26367	28201
		FGOALS-g2	13274	17483	19410	21414	24185	26373	28639	31750	34189
		GFDL-ESM2G	11885	14643	15849	17073	18719	19986	21271	22996	24321
		HadGEM12-ES	11751	14857	16231	17634	19529	20994	22482	24482	26017
		IPSL-CM5A-LR	11223	14025	15228	16436	18044	19268	20499	22135	23379
		MIROC5	12148	15744	17349	18996	21241	22989	24779	27205	29084
		MPI-ESM-LR	11300	14098	15273	16441	17977	19135	20290	21815	22966
		MRI-CGCM3	11326	13855	14912	15959	17331	18363	19391	20743	21762
		NorESM1-M	11852	15044	16446	17873	19796	21281	22789	24817	26377
	2071-2098	BCC-CSM1.1(m)	11075	13679	14775	15864	17298	18380	19460	20885	21961
		BNU-ESM	11804	14566	15707	16831	18298	19396	20485	21914	22987
		CanESM2	11692	14790	16134	17493	19311	20705	22113	23995	25432
		CCSM4	11327	13579	14498	15397	16562	17429	18284	19400	20236
		CNRM-CM5	11915	14693	15872	17048	18602	19779	20957	22515	23695
		CSIRO-Mk3.6.0	11903	14862	16119	17375	19037	20297	21558	23229	24495
		FGOALS-g2	12590	15970	17451	18956	20982	22540	24120	26238	27861
		GFDL-ESM2G	12236	14975	16122	17259	18750	19872	20990	22461	23570
		HadGEM12-ES	11635	14739	16118	17527	19437	20914	22418	24444	26001
		IPSL-CM5A-LR	11380	14208	15387	16554	18084	19234	20378	21884	23018
		MIROC5	11504	14647	16017	17406	19271	20704	22155	24099	25587
		MPI-ESM-LR	11721	14774	16080	17389	19129	20453	21784	23552	24897
		MRI-CGCM3	11208	13714	14766	15811	17185	18220	19252	20614	21641
		NorESM1-M	11884	14763	15990	17217	18844	20079	21318	22961	24207
RCP4.5	2011-2040	ACCESS1.0	11395	13855	14892	15924	17285	18311	19337	20691	21715
		BCC-CSM1.1(m)	11779	14559	15757	16962	18570	19797	21033	22680	23935
		BNU-ESM	11571	14712	16062	17419	19228	20608	21998	23850	25262
		CanESM2	11457	14139	15272	16402	17893	19020	20147	21637	22764
		CCSM4	10389	12510	13416	14322	15524	16436	17351	18564	19485

Scenario	Future period	GCM	Quantile Discharge for return periods (m^3/s)								
			10	50	100	200	500	1000	2000	5000	10000
		CMCC-CM	11728	14434	15576	16713	18213	19346	20478	21974	23105
		CNRM-CM5	11550	14459	15719	16989	18687	19984	21292	23034	24362
		CSIRO-Mk3.6.0	12340	15384	16647	17895	19526	20749	21964	23561	24762
		EC-EARTH	11768	14645	15912	17201	18941	20282	21643	23473	24876
		FGOALS-g2	12241	15284	16595	17915	19674	21016	22367	24166	25535
		GFDL-ESM2G	12002	14534	15570	16586	17904	18885	19854	21119	22066
		HadGEM12-CC	11727	14548	15747	16945	18530	19730	20933	22524	23729
		INM-CM4	11530	14013	15062	16108	17487	18529	19570	20946	21987
		IPSL-CM5A-LR	11463	14397	15658	16925	18614	19902	21199	22925	24239
		MIROC5	10984	14026	15369	16738	18590	20022	21479	23441	24951
		MPI-ESM-LR	10995	13304	14239	15151	16328	17201	18061	19182	20020
		MRI-CGCM3	11382	14158	15381	16627	18312	19614	20940	22727	24103
		NorESM1-M	11627	14983	16479	18012	20099	21721	23382	25631	27371
	2041-2070	ACCESS1.0	10827	13492	14625	15758	17258	18397	19539	21053	22202
		BCC-CSM1.1(m)	12300	15416	16761	18118	19929	21315	22712	24577	26000
		BNU-ESM	10860	13753	14987	16223	17863	19110	20362	22024	23287
		CanESM2	11192	14185	15503	16845	18657	20057	21480	23396	24868
		CCSM4	11089	13508	14512	15504	16800	17772	18737	20003	20956
		CMCC-CM	12170	15065	16292	17515	19130	20353	21576	23195	24420
		CNRM-CM5	11045	13755	14934	16127	17724	18948	20183	21833	23091
		CSIRO-Mk3.6.0	11487	14400	15654	16917	18600	19886	21180	22905	24220
		EC-EARTH	12227	15166	16440	17726	19445	20761	22087	23858	25208
		FGOALS-g2	12416	15483	16795	18109	19854	21181	22512	24279	25620
		GFDL-ESM2G	12334	15317	16590	17864	19555	20840	22130	23844	25145
		HadGEM12-CC	11526	15085	16691	18349	20622	22401	24230	26720	28656
		INM-CM4	11359	14215	15456	16712	18396	19690	21001	22757	24105
		IPSL-CM5A-LR	11170	14421	15829	17250	19154	20613	22087	24058	25565
		MIROC5	12189	15883	17497	19136	21343	23042	24766	27080	28855
		MPI-ESM-LR	10747	13447	14591	15732	17241	18384	19528	21044	22192
		MRI-CGCM3	11510	14282	15472	16666	18257	19469	20689	22312	23547
		NorESM1-M	11415	14539	15915	17316	19209	20672	22159	24160	25700
	2071-2100	ACCESS1.0	11184	13788	14834	15851	17159	18127	19078	20316	21238
		BCC-CSM1.1(m)	11035	13891	15099	16305	17898	19103	20309	21906	23114
		BNU-ESM	11582	15353	17021	18726	21041	22838	24675	27163	29089
		CanESM2	11797	15293	16828	18390	20498	22126	23780	26007	27719
		CCSM4	10446	12850	13877	14905	16269	17306	18347	19730	20780
		CMCC-CM	12566	16017	17513	19024	21048	22600	24170	26271	27880
		CNRM-CM5	11792	15291	16873	18506	20745	22499	24302	26759	28669
		CSIRO-Mk3.6.0	11870	14966	16286	17608	19362	20694	22030	23804	25150
		EC-EARTH	11812	14617	15816	17018	18612	19824	21040	22654	23878
		FGOALS-g2	13551	17395	19145	20960	23460	25426	27455	30232	32402
		GFDL-ESM2G	12521	15601	16902	18198	19909	21202	22495	24204	25498
		HadGEM12-CC	11957	15144	16528	17927	19799	21233	22681	24614	26088
		INM-CM4	11419	14146	15277	16393	17850	18942	20025	21446	22513
		IPSL-CM5A-LR	11403	14576	15937	17305	19126	20513	21910	23769	25184
		MIROC5	11502	14376	15576	16767	18330	19506	20678	22222	23387
		MPI-ESM-LR	11352	14002	15087	16150	17530	18558	19574	20902	21897
		MRI-CGCM3	10798	13364	14451	15537	16972	18059	19147	20587	21679
		NorESM1-M	11371	14398	15723	17069	18882	20277	21692	23592	25049
RCP8.5	2011-	ACCESS1.0	10431	12929	14012	15106	16570	17692	18824	20337	21493

Scenario	Future period	GCM	Quantile Discharge for return periods (m^3/s)								
			10	50	100	200	500	1000	2000	5000	10000
	2040	BCC-CSM1.1(m)	11055	13443	14445	15439	16744	17728	18708	20000	20974
		BNU-ESM	10955	13892	15163	16446	18162	19476	20804	22579	23936
		CanESM2	11162	14114	15424	16765	18584	19995	21434	23379	24879
		CCSM4	11013	13822	15042	16277	17934	19206	20493	22219	23541
		CMCC-CM	12634	15695	16994	18291	20005	21304	22605	24327	25631
		CNRM-CM5	11112	13933	15164	16413	18088	19374	20675	22415	23745
		CSIRO-Mk3.6.0	11951	14968	16290	17632	19437	20827	22237	24128	25578
		EC-EARTH	11553	14130	15238	16352	17835	18965	20101	21612	22761
		FGOALS-g2	11201	13835	14973	16118	17647	18814	19990	21556	22750
		GFDL-ESM2G	11743	14301	15344	16363	17683	18664	19632	20895	21840
		HadGEM12-CC	11073	13939	15204	16492	18231	19571	20932	22759	24159
		INM-CM4	11246	13702	14718	15718	17023	17998	18965	20231	21180
		IPSL-CM5A-LR	10602	13287	14451	15625	17197	18401	19616	21239	22478
		MIROC5	10576	13463	14775	16134	18001	19467	20978	23041	24650
		MPI-ESM-LR	11525	14433	15625	16795	18315	19449	20571	22039	23139
		MRI-CGCM3	10889	13469	14595	15736	17269	18447	19640	21240	22467
		NorESM1-M	12475	15561	16870	18176	19903	21211	22520	24252	25564
	2041-2070	ACCESS1.0	10542	13324	14522	15727	17335	18563	19801	21452	22711
		BCC-CSM1.1(m)	11564	14340	15512	16680	18219	19382	20545	22081	23243
		BNU-ESM	10658	13800	15169	16557	18423	19858	21315	23270	24770
		CanESM2	10635	13567	14857	16172	17948	19320	20714	22592	24036
		CCSM4	10304	12547	13482	14408	15620	16530	17436	18627	19524
		CMCC-CM	13116	16364	17728	19082	20863	22206	23545	25311	26643
		CNRM-CM5	11738	14908	16319	17763	19722	21242	22792	24884	26497
		CSIRO-Mk3.6.0	12083	15344	16762	18196	20120	21596	23089	25086	26614
		EC-EARTH	11452	14208	15396	16592	18186	19402	20627	22258	23500
		FGOALS-g2	12866	16822	18618	20479	23043	25061	27145	30000	32233
		GFDL-ESM2G	11440	14160	15306	16446	17948	19082	20215	21710	22840
		HadGEM12-CC	11113	14185	15527	16887	18713	20116	21534	23432	24882
		INM-CM4	10991	13412	14403	15373	16630	17565	18488	19692	20592
		IPSL-CM5A-LR	10337	13318	14624	15950	17738	19115	20514	22394	23837
		MIROC5	11495	14652	16027	17419	19287	20722	22174	24117	25605
		MPI-ESM-LR	10801	13624	14819	16009	17582	18771	19961	21535	22726
		MRI-CGCM3	10350	12743	13757	14768	16105	17117	18129	19469	20484
		NorESM1-M	12008	15206	16582	17965	19808	21214	22629	24513	25947
	2071-2098	ACCESS1.0	9996	12908	14164	15430	17121	18415	19721	21466	22799
		BCC-CSM1.1(m)	11680	15432	17147	18933	21409	23369	25405	28215	30429
		BNU-ESM	11196	14915	16576	18284	20616	22438	24310	26859	28843
		CanESM2	10496	14464	16315	18264	21000	23194	25497	28710	31270
		CCSM4	10329	13161	14393	15640	17315	18602	19907	21657	23000
		CMCC-CM	13645	18255	20370	22578	25645	28081	30618	34129	36903
		CNRM-CM5	11122	14807	16514	18303	20796	22781	24850	27712	29973
		CSIRO-Mk3.6.0	11858	15739	17497	19319	21826	23798	25836	28626	30810
		EC-EARTH	12071	15858	17559	19313	21715	23594	25526	28159	30209
		FGOALS-g2	13587	17577	19340	21139	23574	25460	27382	29975	31975
		GFDL-ESM2G	11274	14481	15873	17281	19171	20623	22094	24065	25577
		HadGEM12-CC	10316	13853	15450	17098	19360	21131	22953	25435	27367
		INM-CM4	10689	13327	14436	15538	16988	18082	19173	20613	21701
		IPSL-CM5A-LR	10926	14093	15454	16824	18649	20043	21446	23315	24739
		MIROC5	10516	13613	14982	16378	18270	19734	21226	23239	24790

Scenario	Future period	GCM	Quantile Discharge for return periods (m^3/s)								
			10	**50**	**100**	**200**	**500**	**1000**	**2000**	**5000**	**10000**
		MPI-ESM-LR	9995	13203	14633	16100	18098	19656	21252	23418	25099
		MRI-CGCM3	10975	14007	15324	16655	18440	19810	21197	23055	24478
		NorESM1-M	11472	14903	16434	18005	20145	21812	23518	25833	27626

APPENDIX C: FIGURES

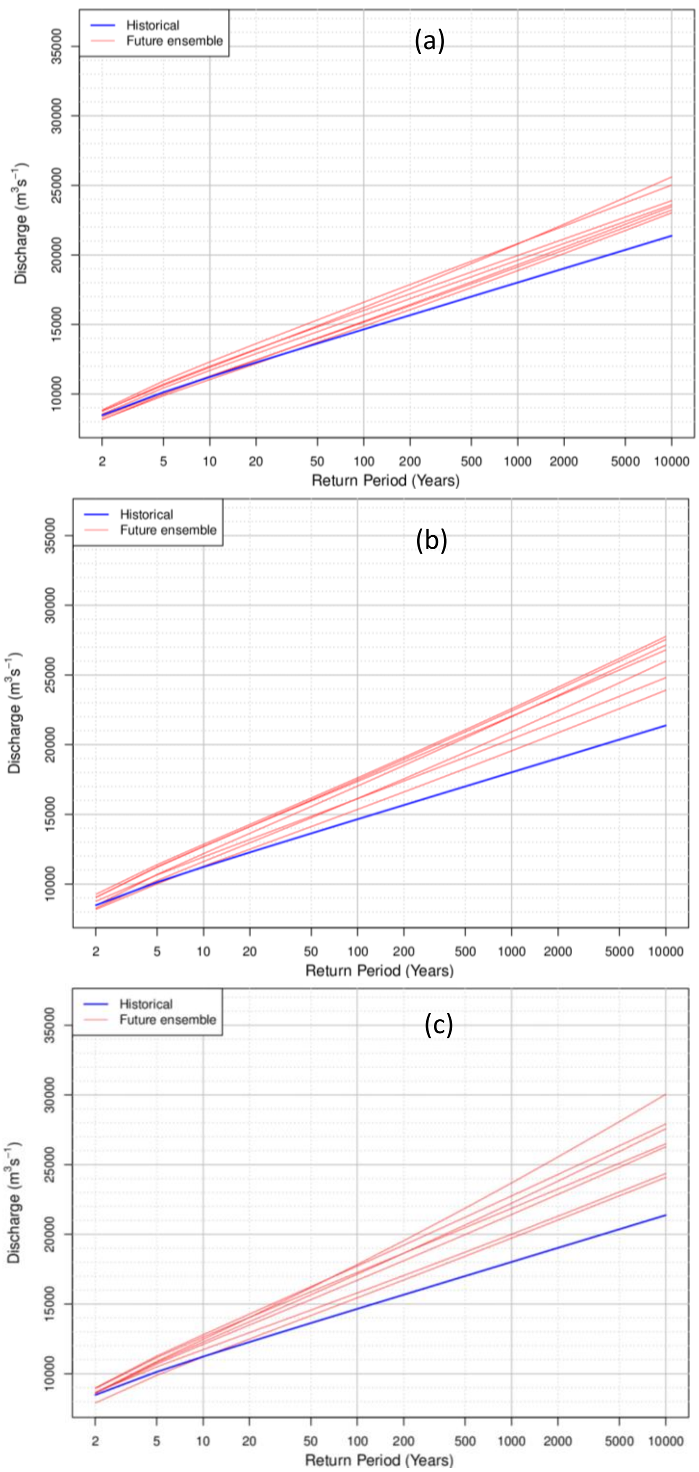

Figure C1. Future (CMIP3 B1 emissions scenarios) flood frequency curves compared to the historical plot for the periods (a) 2011-2040; (b) 2041-2070; and (c) 2071-2100.

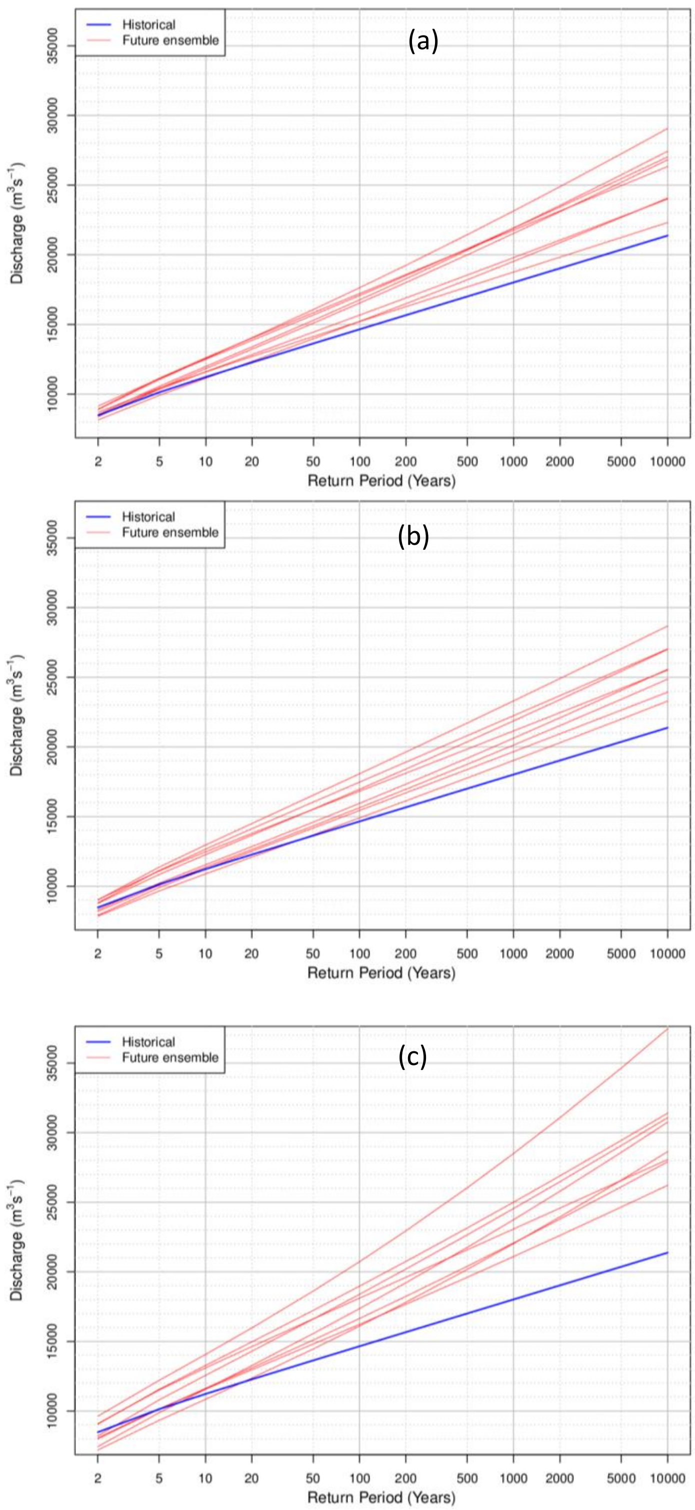

Figure C2. . Future (CMIP3 A2 emissions scenarios) flood frequency curves compared to the historical plot for the periods (a) 2011-2040; (b) 2041-2070; and (c) 2071-2100.

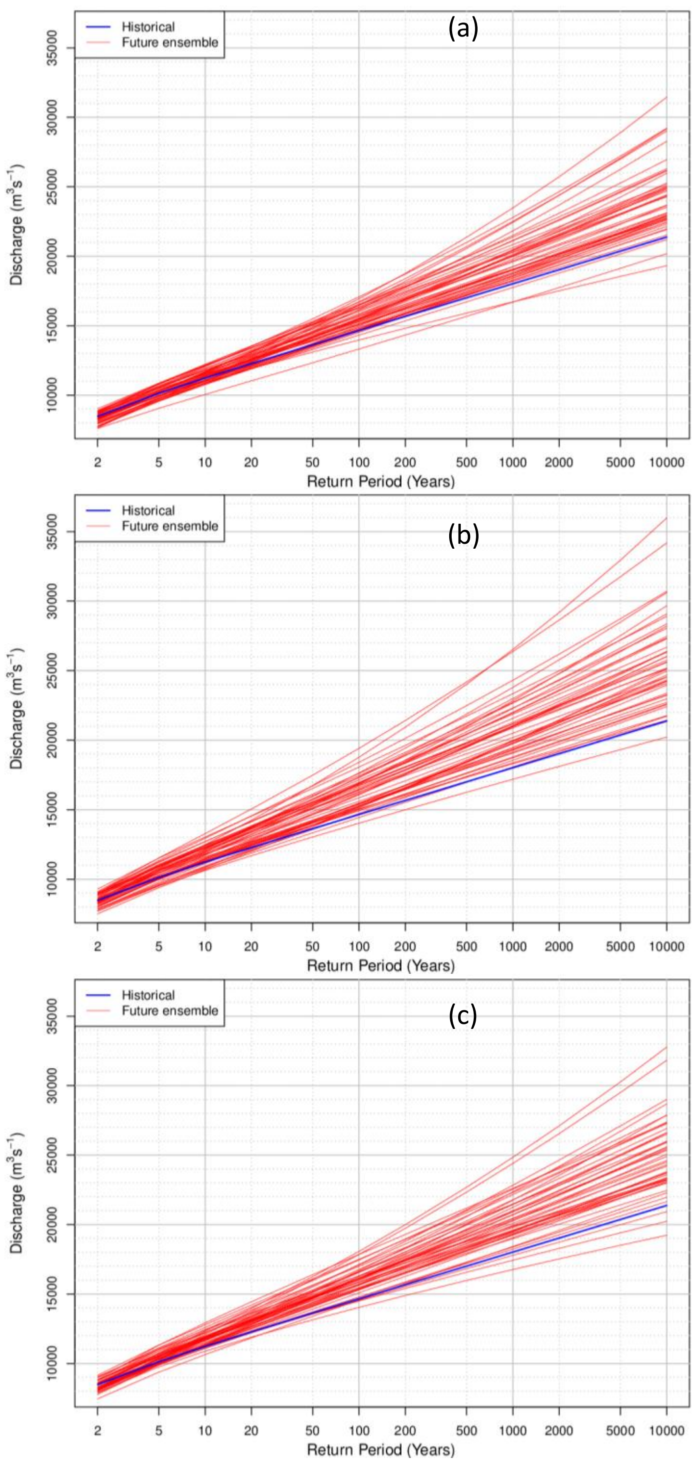

Figure C3. Future (CMIP5 RCP2.6) flood frequency curves compared to the historical plot for the periods (a) 2011-2040; (b) 2041-2070; and (c) 2071-2100.

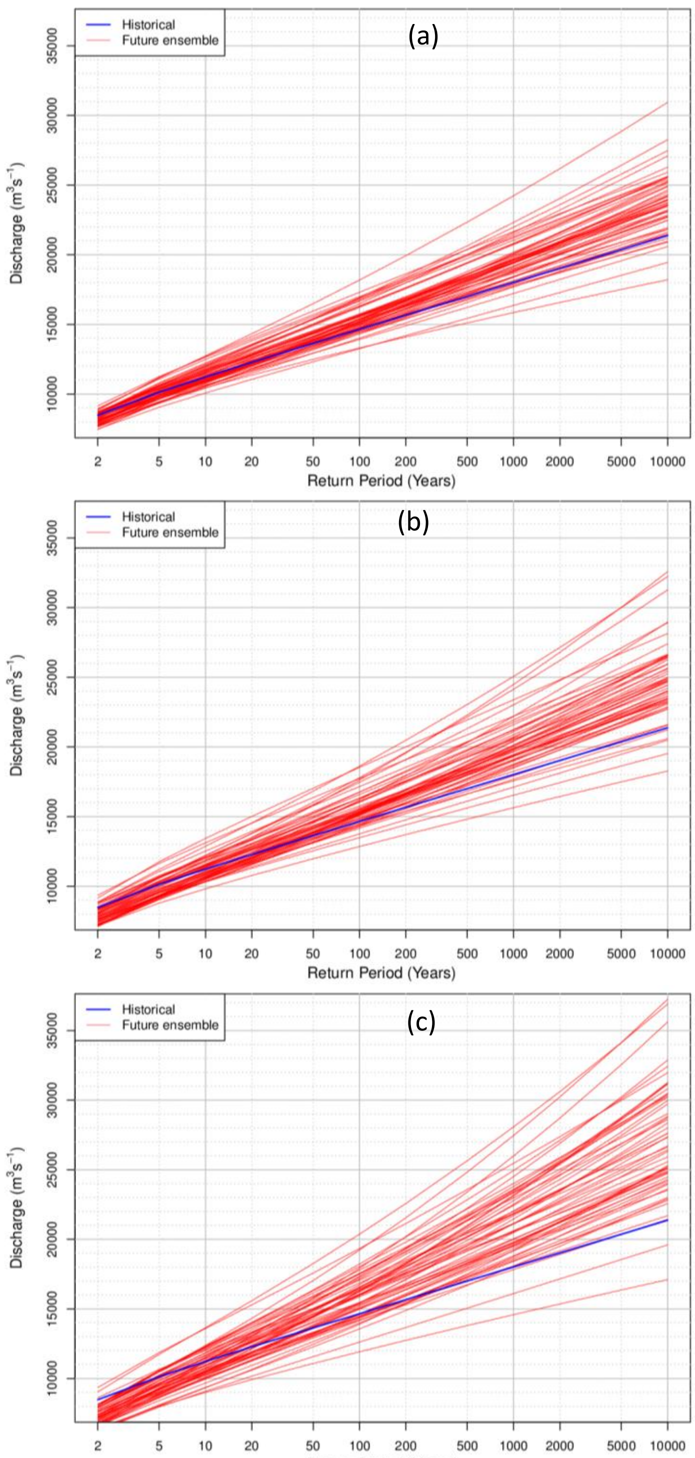

Figure C4. . Future (CMIP5 RCP8.5) flood frequency curves compared to the historical plot for the periods (a) 2011-2040; (b) 2041-2070; and (c) 2071-2100